EFFECT OF PRESTRESSED FIBERS UPON THE RESPONSE OF COMPOSITE MATERIALS

Thesis

Submitted to School of Engineering of the

UNIVERSITY OF DAYTON

In Partial Fulfillment of the Requirements for

The Degree

Masters of Science in Mechanical Engineering

David H. Rose

UNIVERSITY OF DAYTON

May 1993

APPROVED BY:

James M. Whitney, Ph.D.
Professor
Department of Materials Engineering
Committee Chairman

Fred K. Bogner, Ph.D.
Chairman
Department of Civil Engineering
Committee Member

Tony E. Saliba, Ph.D.
Associate Professor
Department of Chemical Engineering
Committee Member

George R. Doyle, Ph.D.
Professor
Department of Mechanical Engineering
Committee Member

Franklin Eastep, Ph.D.
Interim Associate Dean/Director
Graduate Engineering and Research
School of Engineering

Joseph Lestingi, D. Eng., P.E.
Dean
School of Engineering

ABSTRACT

EFFECT OF PRESTRESSED FIBERS UPON THE RESPONSE OF COMPOSITE MATERIALS

Name: Rose, David H.
University of Dayton, 1993

Advisor: Dr. J. M. Whitney

Prestressing materials in order to improve structural characteristics is a common engineering practice. Probably the most evident case is the use of prestressed concrete. This class of material is utilized in situations where the structure is loaded in tension. The prestress is obtained by using steel wires which are loaded in tension prior to the curing of the concrete. When the load is released, the brittle concrete is compressed, allowing for the superposition of externally applied tension.

An analog to prestressed concrete has been developed by the author for use with advanced composite materials. However, the goals of this new method of composite fabrication are different than with concrete. The difference in thermal expansion coefficients of the matrix and fibers as well as a large change in temperature following cure result in three dimensional residual stresses. Applying an external load to the fibers during the cure cycle is seen as a means of both mitigating these stresses as well as prescribing a greater degree of fiber linearity within the composite.

The effect of applying stresses to the fibers prior to consolidation is determined through both mathematical and experimental techniques. A boundary value problem is posed utilizing an elasticity method based on a concentric cylinder model. This model allows for the prediction of the stress/strain state at any point away from the ends of the

laminate. The results obtained from the boundary value problem are used with classical laminated plate theory in order to determine the ply stresses as a function of fiber prestress levels. The experimental procedure includes both the fabrication and mechanical testing of prestressed laminates as well as comparison to data obtained from conventionally processed composites.

ACKNOWLEDGMENTS

I would like to thank my advisor, Dr. James Whitney and supervisor, Scott Theibert for giving me the freedom to conceive of and implement the research program described in this document. I would also like to thank Dr. Nicholas Pagano for his invaluable contributions in helping me to develop the model and to John Camping for his help in fabricating and testing the required specimens. Finally, I would like to thank Barb Hager for providing the graphics and proofreading the manuscript.

TABLE OF CONTENTS

LIST OF ILLUSTRATIONS

LIST OF TABLES

CHAPTER I

INTRODUCTION

Past efforts in characterizing the effect of prestressing fibers prior to laminate consolidation have mostly been accomplished with the intent of increasing specific laminate strength through the fracturing of pre-existing flaws within the fibers [1-5]. This fracturing leads to a better statistical sampling in test specimens as well as a slight increase in strength. This occurs through the elimination of failure inducing mechanisms, such as stress waves, which occur in the vicinity of premature fiber fractures. Other efforts in the area have focused on analyzing the ply stresses induced into the laminate through the prestressing of the fibers as well as determining the impact on the residual stresses using a modified form of classical lamination theory [6]. This work forms the basis for the present effort.

There have been few attempts at fabricating composites in which the fibers have been stressed prior to and during laminate consolidation. The only previous composites fashioned in this manner were prestressed thin specimens obtained by hanging weights on fiber bundles and casting resin around them using a mold [2] or by clamping and stretching the outer layers of a cross ply laminate [7]. In this current effort, filament winding and thermal expansion have been used as a mechanism for prestressing the fibers in unidirectional and crossply laminates. The impetus for the application of this prestress is not to fracture pre-existing flaws in the fibers, although this may be a secondary benefit. What is being proposed is to utilize prestressed fibers in laminated plates as a means of modifying the thermal residual stresses. An additional benefit to holding the fibers under tension prior to laminate consolidation is that the fibers in the bundles should have a smaller

degree of waviness. This feature potentially has an impact in improving the strength of composites.

Analysis of the residual stresses in a typical graphite epoxy composite indicates that the longitudinal matrix stress is tensile in nature and of considerable magnitude. Depending on the actual fibers and matrix materials used, this stress can equate to roughly 50% of the tensile strength of the neat epoxy resin. By prestressing the fibers prior to laminate consolidation and then releasing the load following cure, a mechanism has been found that can reduce the magnitude of the longitudinal tensile stress in the matrix and the associated strain. The relative advantage to modifying the stress field is it provides a means of both delaying the onset of matrix cracking as well as allowing for an increase in applied external loading.

CHAPTER II

LITERATURE REVIEW

A review of the literature indicated little research has been conducted in the area of prestressed composites. Of the limited number of papers available, the earliest were by Manders and Chou [1] and Chi and Chou [3]. The relevance of this work to the present is minimal since their objective was to stress the fibers prior to but not during the cure cycle. They hypothesized that applying a stress prior to laminate consolidation would fracture the fibers at the points where flaws exist. It was speculated that by eliminating the flaws, the tendency for the fibers to rupture under low loading conditions would be significantly reduced. Even though the stress in these fibers at fracture is low, the energy associated with the stress is immediately released. This creates a dynamic event resulting in stress waves which radiate out from the fracture. These stress waves induce other undamaged fibers to prematurely fail. The results of the experimental work conducted by Manders and Chou showed that applying a stress prior to laminate consolidation yielded a composite with minimal increases in strength. However, it was shown that the variability in composite strength was significantly reduced as a result of the elimination of the low load level dynamic events.

In later work, Tuttle [6] formulated an analytical approach for predicting the response of prestressed composite laminates under prescribed loading conditions. This work represented the first attempt at understanding the effect of prestressing upon the load carrying capability of a composite. In this analysis, it was specified that the fibers were held under tension during the cure cycle. It was demonstrated that prestressing caused a

modification of the residual stresses which normally result from the cooling of a composite. In order to simplify the model, it was assumed that the matrix and fibers were isotropic linearly elastic materials. One point made by Tuttle was that tailoring the prestress applied to the fiber can result in a composite in which the tensile residual stresses found in the matrix can be eliminated.

Perhaps the first demonstrated fabrication process was shown by Jorge, Marques, and De Castro [2]. The technique they developed for applying tension to the fiber tow was to alternate the tow back and forth between sets of steel pins and to have tension applied at the tow end. Once the fibers were under tension, a liquid polyester resin was applied and the fibers and resin were sandwiched between glass plates. Pressure was then applied to the plates in order to consolidate the laminate. Narrow unidirectional specimens were obtained from this process. Mechanical testing of these specimens indicated that composite strength increased slightly with increasing prestress level. They also showed that the modulus of the specimens increased. Fractographic analyses using a scanning electron microscope were conducted on the fracture surfaces of both prestressed and conventionally processed specimens. They observed there were no apparent differences in the appearance of the fracture surfaces of the different specimens.

The final paper appeared in the literature late in the development of this current work. This paper by Schulte and Marrissen [7] has some common features with the work being presented here. The obvious similarity is the fabrication of crossply prestressed laminates. They point out that the benefit of prestressing is seen in the tendency for prestressed laminates to undergo higher levels of strain before the first matrix cracks appear. Since designs are dictated by the maximum amount of strain allowed, the authors state that the obvious benefit of prestressing composites is structures can then be designed to take higher amounts of applied strain. This means that less material can be used resulting in both an economic advantage as well as increased performance.

The method they used to fabricate the prestressed laminate was to construct a fixture which had two features: one of which was the ability to clamp the prepreg tightly at the ends and the other was the ability to apply tension to the fibers by clamping a bar over the prepreg and forcing it down into a v-notch machined into the surface of the fixture. Forcing prepreg into a notch under pressure is an arduous task. Due to the severity of this operation, the fibers being stressed had to be tolerant of severe handling conditions without fracturing. For these reasons, aramid/epoxy prepreg was chosen for use in the outer layers. The construction details of the fixture precluded the application of tension to the inner layers. Since these layers were not tensioned, carbon/epoxy prepreg was used. The end result of this process was a hybrid laminate with only the outer layers prestressed.

CHAPTER III

PRESTRESSED COMPOSITE CONCENTRIC CYLINDER MODEL

1. PRELOAD STRAIN DETERMINATION:

The following model is based upon the concentric cylinder approach commonly used for micromechanical analysis of composite materials [9]. The model composite consists of three distinct phases (see Figure 3.1).

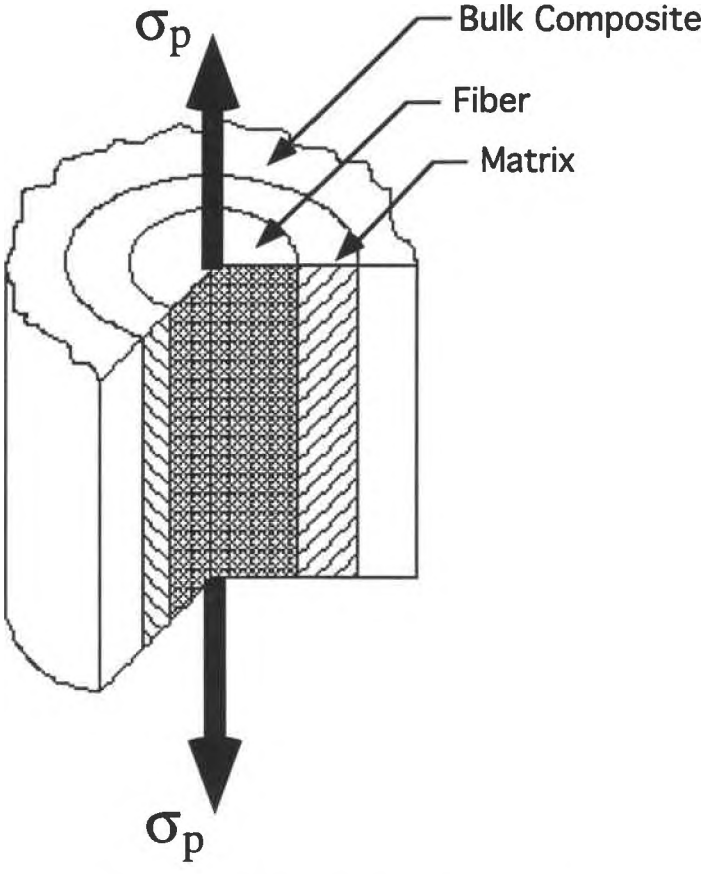

Figure 3.1 Concentric Cylinder Model

The phases represented are a cylindrical fiber overlapped with a cylindrical matrix which is further overwrapped by an unbounded region consisting of a bulk composite with the same properties as the effective properties of the concentric cylinders. The radius of the fiber and matrix cylinders (R_f and R respectively) are such that the volumes of each represent appropriate composite fiber and matrix volumes. The current variation differs in that an external stress, σ_p, is applied to the fibers prior to the solidification of the matrix. This is done in order to change the residual stresses present within the composite following completion of processing.

During the initial portion of the cure cycle, the matrix resin can be considered a viscous fluid while the fibers and mandrel experience thermal expansion. After the mandrel/fiber system has attained equilibrium at the processing temperature, a force balance exists between the fibers and the mandrel. These internal forces are caused by the difference in the thermal expansion coefficients of the fibers and mandrel. The mandrel is chosen such that its coefficient of thermal expansion (CTE) is much greater than the fibers in order for the internal forces to be maximized. The mandrel/fiber force balance can be represented by

$$F_{fiber} + F_{mandrel} = 0 \tag{3.1}$$

For the purpose of this analysis as well as subsequent experiments, the mandrel will be constructed of aluminum in order to benefit from its large CTE. Equation 3.1 can be rewritten in terms of the axial normal stresses

$$\sigma_1^f A_f + \sigma_1^a A_a = 0 \tag{3.2}$$

where the "f" refers to the fibers, "a" the aluminum mandrel, and "1" denotes the axis parallel to the fiber direction. The area, A_f, can be written as

$$A_f = t_p N V_f W_u \tag{3.3}$$

where t_p is the laminate ply thickness, N is the number of plies, V_f is the fiber volume fraction, and W_u is the width (= unity). The mandrel area, A_a can be represented by

$$A_a = t_a W_u \tag{3.4}$$

where t_a is the half thickness of the mandrel. The half thickness is required since the fibers will be stretched on both the top and bottom of the mandrel (see Figure 3.2).

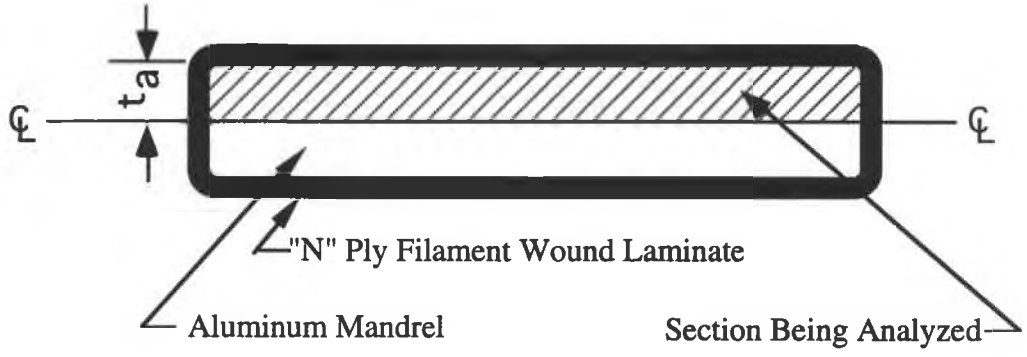

Figure 3.2 Filament Wound Mandrel Cross-section

Since the matrix during the initial portion of the cure cycle is a viscous fluid, the fibers can be assumed to be traction free everywhere except at the ends. This assumption allows the stresses, including the thermal expansion terms, to be rewritten using Hooke's Law

$$\begin{aligned} \sigma_1^f &= E_1^f(\varepsilon_1^f - \alpha_1^f \Delta T_1) \\ \sigma_1^a &= E^a(\varepsilon_1^a - \alpha^a \Delta T_1) \end{aligned} \tag{3.5}$$

where E_1^f is the fiber longitudinal Young's Modulus, E^a is the modulus of the mandrel, ΔT_1 is the difference between the cure and ambient temperatures, α^a is the mandrel

coefficient of thermal expansion (CTE) and α_1^f is the fiber longitudinal CTE. Substituting 3.3, 3.4, and 3.5 into 3.2 and recognizing that ε_1^f equals ε_1^a (= ε_o) allows another form of the force-balance equation.

$$E_1^f t_p N V_f(\varepsilon_o - \alpha_1^f \Delta T_1) = -E^a t_a(\varepsilon_o - \alpha^a \Delta T_1) \tag{3.6}$$

where ε_o is defined as the mechanical strain induced by the expansion of the fiber/mandrel system. Solving 3.6 for ε_o allows for an expression for the "prestrain" induced into the fibers as a result of the thermal processing

$$\varepsilon_o = \frac{(E_1^f t_p N V_f \alpha_1^f + E^a t_a \alpha^a)\Delta T_1}{E_1^f t_p N V_f + E^a t_a} \tag{3.7}$$

This strain corresponds to a unidirectional winding around the mandrel. If we consider the use of a rectangular mandrel so that the fibers can be wound in mutually orthogonal directions, the mandrel constitutive equation takes the following form

$$\frac{1}{E^a}(\sigma_1^a - \nu^a \sigma_2^a) = (\varepsilon_1^a - \alpha^a \Delta T_1) \tag{3.8}$$

where the "1" and "2" subscripts correspond to the coordinate axes parallel to the major dimensions of the mandrel and ν^a refers to the poissons ratio of the mandrel. If the mandrel is square and the same number of layers are wound in each direction, then $\sigma_1 = \sigma_2$. Substituting this into 3.8 and solving for σ_1 yields the following

$$\sigma_1^a = \frac{(\varepsilon_1^a - \alpha^a \Delta T_1)E^a}{(1 - \nu^a)} \tag{3.9}$$

Substituting this for the corresponding expression in Equations 3.5 and using 3.3 and 3.4 along with 3.2 yields the strain induced into the fibers of a crossply laminate as a result of filament winding and thermal expansion.

$$\varepsilon_o = \frac{(E_1^f t_p N V_f \alpha_1^f (1-\nu^a) + E^a t_a \alpha^a)\Delta T_l}{E_1^f t_p N V_f (1-\nu^a) + E^a t_a} \tag{3.10}$$

Other levels of prestress can be analyzed through the following relationship

$$\sigma_p = \varepsilon_o E_1^f \tag{3.11}$$

which can be rewritten to solve for the applied prestrain in terms of an applied stress.

$$\varepsilon_o = \frac{\sigma_p}{E_1^f} \tag{3.12}$$

2. CONSTITUTIVE EQUATION DETERMINATION:

The strains that exist in the fibers and matrix subsequent to process completion are a result of the applied "prestrain" as well as the strain contribution due to cool-down shrinkage. A force balance is required within the composite to ensure equilibrium of internal forces after the relaxation of the external thermal load. ε_1^f and ε_1^m are defined as the overall longitudinal fiber and matrix strains resulting from the release of the thermal loading. Interface continuity between the fiber and the matrix leads to the assumption that these strains are equal

$$\varepsilon_1^f = \varepsilon_1^m = \varepsilon_1 \tag{3.13}$$

The fiber strains can be written in the following fashion

$$\begin{aligned}\varepsilon^f_1 &= -\varepsilon_o + \alpha^f_1\Delta T_2 + S^f{}_{1i}\sigma^f{}_i \\ \varepsilon^f_2 &= +\nu^f_{12}\varepsilon_o + \alpha^f_2\Delta T_2 + S^f{}_{2i}\sigma^f{}_i \\ \varepsilon^f_3 &= +\nu^f_{13}\varepsilon_o + \alpha^f_3\Delta T_2 + S^f{}_{3i}\sigma^f{}_i\end{aligned} \tag{3.14}$$

where ε_0 is the applied thermally induced strain, the $\alpha\Delta T_2$ term is the strain contribution due to the cool-down cycle, $S^f_{ij}\sigma^f_j$ are the mechanical fiber strains resulting from the internal force balance, and the 1,2,3 subscripts correspond to the z,r,θ cylindrical coordinates. In a similar fashion, the strain induced into the matrix upon the release of the applied load can be determined.

$$\varepsilon^m_i = S^m_{ij}\sigma^m_j + \alpha^m_i\Delta T_2 \tag{3.15}$$

In both 3.14 and 3.15, ΔT_2 is defined as the change in temperature from the cure temperature to some other "use" temperature. If the fiber is assumed to be transversely isotropic, then $\nu^f{}_{12} = \nu^f{}_{13}$ which allows algebraic manipulation and matrix inversion to be used on 3.14, thus yielding

$$\sigma^f_i = C^f_{ij}(\varepsilon^f_j - e_j - \alpha^f_j\Delta T_2) \qquad i,j = 1,2,3 \tag{3.16}$$

with

$$\begin{aligned}e_1 &= -\varepsilon_o \\ e_2 &= e_3 = \nu^f_{12}\varepsilon_o\end{aligned} \tag{3.17}$$

Likewise, 3.15 can be operated on to determine the matrix constitutive equations

$$\sigma_i^m = C_{ij}^m(\varepsilon_j^m - \alpha_j^m \Delta T_2) \qquad i,j = 1,2,3 \tag{3.18}$$

Assuming transversely isotropic behavior, using cylindrical coordinate notation and substituting 3.13 and 3.14 allows 3.16 to be expanded and simplified

$$\begin{aligned}
\sigma_z^f &= C_{11}^f(\varepsilon_z + \varepsilon_o - \alpha_1^f \Delta T_2) + C_{12}^f(\varepsilon_r^f + \varepsilon_\theta^f - 2(\nu_{12}^f \varepsilon_o + \alpha_2^f \Delta T_2)) \\
\sigma_r^f &= C_{12}^f(\varepsilon_z + \varepsilon_o - \alpha_1^f \Delta T_2) + C_{22}^f \varepsilon_r^f + C_{23}^f \varepsilon_\theta^f - (\nu_{12}^f \varepsilon_o + \alpha_2^f \Delta T_2)(C_{22}^f + C_{23}^f) \\
\sigma_\theta^f &= C_{12}^f(\varepsilon_z + \varepsilon_o - \alpha_1^f \Delta T_2) + C_{23}^f \varepsilon_r^f + C_{22}^f \varepsilon_\theta^f - (\nu_{12}^f \varepsilon_o + \alpha_2^f \Delta T_2)(C_{22}^f + C_{23}^f)
\end{aligned} \tag{3.19}$$

where the unknowns are ε_z, ε_r^f, ε_θ^f, σ_z^f, σ_r^f, and σ_θ^f. Equations 3.18 can also be expanded and simplified using isotropic material properties and cylindrical coordinates.

$$\begin{aligned}
\sigma_z^m &= C_{11}^m(\varepsilon_z - \alpha^m \Delta T_2) + C_{12}^m(\varepsilon_r^m + \varepsilon_\theta^m - 2\alpha^m \Delta T_2) \\
\sigma_r^m &= C_{11}^m(\varepsilon_r^m - \alpha^m \Delta T_2) + C_{12}^m(\varepsilon_z + \varepsilon_\theta^m - 2\alpha^m \Delta T_2) \\
\sigma_\theta^m &= C_{11}^m(\varepsilon_\theta^m - \alpha^m \Delta T_2) + C_{12}^m(\varepsilon_z + \varepsilon_r^m - 2\alpha^m \Delta T_2)
\end{aligned} \tag{3.20}$$

where the unknowns are ε_z, ε_r^m, ε_θ^m, σ_z^m, σ_r^m, and σ_θ^m.

3. DETERMINATION OF THE STRAINS AND DISPLACEMENTS :

The radial and circumferential displacements in the fiber can be assumed to be of the following form

$$u_r^f = F_1(r) \qquad u_\theta^f = 0 \tag{3.21}$$

while those in the matrix are of similar form

$$u_r^m = F_2(r) \qquad u_\theta^m = 0 \tag{3.22}$$

Interface continuity requires that

$$u_r^f(R_f) = u_r^m(R_f) \tag{3.23}$$

where R_f is the fiber radius. The strain displacement relations [10]

$$\varepsilon_r = \frac{\partial u_r}{\partial r} \qquad \varepsilon_\theta = \frac{u_r}{r} \tag{3.24}$$

can be used with 3.21 and 3.22 to obtain the assumed states of strain in the fiber

$$\varepsilon_r^f = \frac{dF_1(r)}{dr} \qquad \varepsilon_\theta^f = \frac{F_1(r)}{r} \tag{3.25}$$

and matrix

$$\varepsilon_r^m = \frac{dF_2(r)}{dr} \qquad \varepsilon_\theta^m = \frac{F_2(r)}{r} \tag{3.26}$$

Using the σ_r^f and σ_θ^f expressions from 3.19 and inserting 3.25

$$\sigma_r^f = C_{12}^f(\varepsilon_z + \varepsilon_o - \alpha_1^f \Delta T_2) + C_{22}^f \frac{dF_1(r)}{dr} + C_{23}^f \frac{F_1(r)}{r} - (\nu_{12}^f \varepsilon_o + \alpha_2^f \Delta T_2)(C_{22}^f + C_{23}^f)$$
$$\sigma_\theta^f = C_{12}^f(\varepsilon_z + \varepsilon_o - \alpha_1^f \Delta T_2) + C_{23}^f \frac{dF_1(r)}{dr} + C_{22}^f \frac{F_1(r)}{r} - (\nu_{12}^f \varepsilon_o + \alpha_2^f \Delta T_2)(C_{22}^f + C_{23}^f) \tag{3.27}$$

Differentiating σ_r^f with respect to r

$$\frac{d\sigma_r^f}{dr} = C_{22}^f \frac{d^2F_1(r)}{dr^2} + C_{23}^f \left(\frac{1}{r} \frac{dF_1(r)}{dr} - \frac{F_1(r)}{r^2} \right) \tag{3.28}$$

Since there are no shear forces, the equilibrium equation reduces to the following general form.

$$\frac{\partial \sigma_r}{\partial r} + \frac{\sigma_r - \sigma_\theta}{r} = 0 \tag{3.29}$$

Inserting 3.27 and 3.28 into 3.29 and reducing gives the following second order differential equation.

$$\frac{d^2F_1(r)}{dr^2} + \frac{1}{r}\frac{dF_1(r)}{dr} - \frac{F_1(r)}{r^2} = 0 \tag{3.30}$$

The solution for this equation is of the form

$$F_1 = a_0 r + \frac{a_1}{r} \tag{3.31}$$

By inspection, the constant a_1 must equal zero in order for F_1 to remain finite at r=0. Therefore,

$$F_1 = a_0 r \tag{3.32}$$

and

$$\frac{dF_1(r)}{dr} = a_0 \tag{3.33}$$

Substituting 3.32 and 3.33 into 3.25 allows for the solution for the strains ε_r^f and ε_θ^f in terms of some unknown constant.

$$\varepsilon_r^f = \varepsilon_\theta^f = a_0 \tag{3.34}$$

Inserting 3.34 into 3.19

$$\sigma_z^f = C_{11}^f(\varepsilon_z + \varepsilon_o - \alpha_1^f \Delta T_2) + 2C_{12}^f(a_0 - \nu_{12}^f \varepsilon_o - \alpha_2^f \Delta T_2)$$
$$\sigma_r^f = \sigma_\theta^f = C_{12}^f(\varepsilon_z + \varepsilon_o - \alpha_1^f \Delta T_2) + (a_0 - \nu_{12}^f \varepsilon_o - \alpha_2^f \Delta T_2)(C_{22}^f + C_{23}^f) \quad (3.35)$$

where Equations 3.35 are written in terms of the unknown coefficient a_o. Equations for the stresses in the matrix are obtained by using the σ_r^m and σ_θ^m expressions from 3.20 and inserting 3.26.

$$\sigma_r^m = C_{11}^m\left(\frac{dF_2(r)}{dr} - \alpha^m \Delta T_2\right) + C_{12}^m\left(\varepsilon_z^m + \frac{F_2(r)}{r} - 2\alpha^m \Delta T_2\right)$$
$$\sigma_\theta^m = C_{11}^m\left(\frac{F_2(r)}{r} - \alpha^m \Delta T_2\right) + C_{12}^m\left(\varepsilon_z^m + \frac{dF_2(r)}{dr} - 2\alpha^m \Delta T_2\right) \quad (3.36)$$

Differentiating σ_r^m with respect to r yields

$$\frac{d\sigma_r^m}{dr} = C_{11}^m \frac{d^2F_2(r)}{dr^2} + C_{12}^m\left(\frac{1}{r}\frac{dF_2(r)}{dr} - \frac{F_2(r)}{r^2}\right) \quad (3.37)$$

Inserting 3.36 and 3.37 into 3.29 yields another 2nd order differential equation

$$\frac{d^2F_2(r)}{dr^2} + \frac{1}{r}\frac{dF_2(r)}{dr} - \frac{F_2(r)}{r^2} = 0 \quad (3.38)$$

where the unknown functions are used for determination of the matrix strains. The solution to 3.38 is of the form

$$F_2(r) = b_0 r + \frac{b_1}{r} \quad (3.39)$$

Substituting 3.39 into 3.26 provides the following expressions for the matrix strains

$$\varepsilon_r^m = b_0 - \frac{b_1}{r^2}$$
$$\varepsilon_\theta^m = b_0 + \frac{b_1}{r^2} \tag{3.40}$$

Equations 3.40 allow 3.20 to be rewritten as

$$\sigma_z^m = C_{11}^m(\varepsilon_z - \alpha^m\Delta T_2) + 2C_{12}^m(b_0 - \alpha^m\Delta T_2)$$
$$\sigma_r^m = (C_{11}^m + C_{12}^m)b_0 + (C_{12}^m - C_{11}^m)\frac{b_1}{r^2} - C_{11}^m\alpha^m\Delta T_2 + C_{12}^m(\varepsilon_z - 2\alpha^m\Delta T_2)$$
$$\sigma_\theta^m = (C_{11}^m + C_{12}^m)b_0 + (C_{11}^m - C_{12}^m)\frac{b_1}{r^2} - C_{11}^m\alpha^m\Delta T_2 + C_{12}^m(\varepsilon_z - 2\alpha^m\Delta T_2) \tag{3. 41}$$

where Equations 3.41 are written in terms of the unknown coefficients ε_z, b_0 and b_1.

Continuity of the radial displacements at the fiber-matrix interface ($r = R_f$) must be maintained. Therefore, Equations 3.21, 3.22, 3.32, and 3.39 can be used with 3.23 to obtain

$$a_0 = b_0 + \frac{b_1}{R_f^2} \tag{3.42}$$

which substituted into 3.35 provides

$$\sigma_z^f = C_{11}^f(\varepsilon_z + \varepsilon_o - \alpha_1^f\Delta T_2) + 2C_{12}^f(b_0 + \frac{b_1}{R_f^2} - \nu_{12}^f\varepsilon_o - \alpha_2^f\Delta T_2)$$
$$\sigma_r^f = \sigma_\theta^f = C_{12}^f(\varepsilon_z + \varepsilon_o - \alpha_1^f\Delta T_2) + (b_0 + \frac{b_1}{R_f^2} - \nu_{12}^f\varepsilon_o - \alpha_2^f\Delta T_2)(C_{22}^f + C_{23}^f) \tag{3.43}$$

4. DETERMINATION OF SIMULTANEOUS EQUATIONS :

Continuity requires the radial stresses at the interface to be equal.

$$\sigma_r^f(R_f) = \sigma_r^m(R_f) \tag{3.44}$$

Using the σ_r^f equation from 3.43 and equating to σ_r^m from 3.41 when $r = R_f$

$$(C_{12}^f - C_{12}^m)\varepsilon_z + (C_{22}^f + C_{23}^f - C_{11}^m - C_{12}^m)b_o + (C_{22}^f + C_{23}^f + C_{11}^m - C_{12}^m)\frac{b_1}{R_f^2}$$
$$= -C_{12}^f(\varepsilon_o - \alpha_1^f\Delta T_2) + (\nu_{12}^f\varepsilon_o + \alpha_2^f\Delta T_2)(C_{22}^f + C_{23}^f) - (C_{11}^m + 2C_{12}^m)\alpha^m\Delta T_2 \tag{3.45}$$

where the unknowns are b_0, b_1, and ε_z. A second expression relating these three terms can be arrived at by analyzing the radial matrix stresses at some point away from the interface

$$\sigma_r^m(R) = 0 \tag{3.46}$$

where R is the radius of the interface between the matrix cylinder and the surrounding homogeneous media. This radius can be determined as a function of the fiber volume fraction.

$$V_f = \frac{\pi R_f^2}{\pi R^2} \tag{3.47}$$

Solving 3.47 for R gives

$$R = \frac{R_f}{\sqrt{V_f}} \tag{3.48}$$

The expression relating the three unknowns can be determined by using the σ_r^m equation from 3.41, setting $r = R$, and equating to zero.

$$C_{12}^m\varepsilon_z + (C_{11}^m + C_{12}^m)b_o + (C_{12}^m - C_{11}^m)\frac{V_f}{R_f^2}b_1 = (C_{11}^m + 2C_{12}^m)\alpha^m\Delta T_2 \tag{3.49}$$

Since there are three unknowns, another expression is required. This equation can be determined through a force balance analysis. After the temperature is reduced, the load induced into the fibers is released and the fibers will contract. The amount of contraction is dependent upon the resistance from the matrix which at this point is no longer a viscous fluid. Therefore, an internal force balance occurs between the fibers and the matrix.

$$F_{fiber} + F_{matrix} = 0 \tag{3.50}$$

Since σ_z^f and σ_z^m are assumed to be independent of r, this expression can be rewritten in the following form

$$\sigma_z^f A_f + \sigma_z^m A_m = 0 \tag{3.51}$$

Where A_f is the area of the fiber and A_m is the matrix area. These can be replaced by the fiber volume

$$\sigma_z^f V_f + \sigma_z^m (1-V_f) = 0 \tag{3.52}$$

The longitudinal stress equations in terms of the unknown coefficients can now be used to determine the third relationship. Substituting the expression for σ_z^f from 3.43 and σ_z^m from 3.41 into 3.52 allows for the derivation of a third equation relating the three unknowns.

$$(C_{11}^f V_f + C_{11}^m(1 - V_f))\varepsilon_z + 2(C_{12}^f V_f + C_{12}^m(1 - V_f))b_o + 2C_{12}^f \frac{V_f}{R_f^2} b_1 =$$
$$\alpha^m \Delta T_2 (C_{11}^m + 2C_{12}^m)(1 - V_f) - (C_{11}^f(\varepsilon_o - \alpha_1^f \Delta T_2) - 2C_{12}^f(\nu_{12}^f \varepsilon_o + \alpha_2^f \Delta T_2))V_f \tag{3.53}$$

The solutions for the unknown coefficients b_0, b_1, and ε_z can now be determined by simultaneously solving Equations 3.45, 3.49, and 3.53. Due to the complexity of these equations, they cannot easily be solved in a closed form. Therefore, the method of solution will be to substitute in values for the various quantities and solve numerically. The values of b_0, b_1, and ε_z can then be used with Equations 3.41 and 3.43 to determine the stresses at any point within the system.

5. ANALYTICAL RESULTS FOR THE AS-4/3501-6 SYSTEM:

Since the solutions to be obtained from the present model are three dimensional, then the 3-D constituent material properties are required. The following are the material properties that are well characterized (Hercules properties).

KNOWN PROPERTIES:

-MATRIX (3501-6 Epoxy):

$$E^m = .62 \times 10^6 \text{ psi}$$

$$\alpha^m = 22.8 \times 10^{-6} \text{ in/in } ^oF$$

$$\nu^m = 0.34$$

-FIBER (AS-4):

$$E_1^f = 34 \times 10^6 \text{ psi}$$

$$\nu_{12}^f = 0.3$$

A common difficulty encountered when trying to determine material properties, particularly for composites, is the variability which exists between specimens. Additionally, the results can vary depending upon the test methods and procedures which were used to obtain the data. For this reason, two sets of laminate CTE properties were obtained, one from the manufacturer and the other which resulted from an independent assessment conducted for

the Materials Directorate (ML), Wright-Patterson AFB, Ohio [11]. These properties are extremely important for the present analysis since the process of prestressing is predicated upon the mismatch in CTE between the fibers and the mandrel. For this reason, both sets of laminate thermal properties were used in order to bound the solution.

-LAMINATE:

ML DATA

$$\alpha_1 = -0.4 \times 10^{-6} \text{ in/in } ^oF$$
$$\alpha_2 = 15.0 \times 10^{-6} \text{ in/in } ^oF$$

HERCULES DATA

$$\alpha_1 = -0.044 \times 10^{-6} \text{ in/in } ^oF$$
$$\alpha_2 = 12.0 \times 10^{-6} \text{ in/in } ^oF$$

The experimental determination of the fiber CTE is extremely difficult. A common method for determining the longitudinal CTE is to back calculate the property using the inverse rule of mixtures along with known laminate properties. The following result from this method.

ML DATA

$$\alpha_1^f = -6.8204 \times 10^{-7} \text{ in/in } ^oF$$

HERCULES DATA

$$\alpha_1^f = -3.2171 \times 10^{-7} \text{ in/in } ^oF$$

Back calculation provides an accurate means of determining the longitudinal CTE but the method provides poor results for determining the transverse CTE. However, it is possible to use the current model with known properties in order to converge on solutions which are representative of the unknown quantity. Unfortunately, there are two other properties which are unknown, the fiber transverse modulus and poissons ratio. Parametric studies were conducted by varying one of the three unknown values while holding the other two fixed (see Appendix II). During the parametric analysis, no prestress was applied to the

fibers so that a conventional laminate was simulated. The hoop strain at the outer cylinder (matrix) radius was evaluated as the various unknown parameters were changed. This strain, when divided by the change in temperature from cure to ambient, provides an equivalent laminate transverse CTE which can be directly compared with the experimentally determined transverse laminate CTE. It was observed during the course of the study that the hoop strain, thus the laminate transverse CTE, was insensitive to changes in both the transverse fiber modulus as well as the poissons ratio. For this reason, values for these were assumed. The following represent these values:

FIBER:

$$\nu_{23}^{f} = .55$$
$$E_{2}^{f} = 2.4 \text{ X } 10^{6} \text{ psi}$$

Once these values were fixed, the parametric analysis was continued by varying the fiber transverse CTE in order to obtain a cylinder thermal hoop strain comparable with that which would be observed from a laminate. The following represent the fiber transverse CTE which allowed a convergence of the analytical solution thermal strains with the experimentally determined laminate thermal strain.

ML DATA

$$\alpha_{2}^{f} = 6.0 \text{ x } 10^{-6} \text{ in/in } ^{o}F$$

HERCULES DATA

$$\alpha_{2}^{f} = 2.0 \text{ x } 10^{-6} \text{ in/in } ^{o}F$$

Once the constituent material properties have been determined, the only other information needed is that relating to the mandrel and laminate properties as well as the processing conditions.

OTHER PROPERTIES:

Mandrel (Aluminum):

$E^a = 10.6 \times 10^6$ psi $\quad \alpha^a = 13.0 \times 10^{-6}$ in/in ^oF

Thickness (t_a) = 0.125 in $\quad \nu^a = .33$

Processing:

$\Delta T_1 = 280\ ^oF$ (change from ambient to processing temperature)

$\Delta T_2 = -280\ ^oF$ (change from processing to ambient temperature)

Laminate:

Volume Fraction (V_f) = .6

Number of Plies = 4

Ply Thickness (t_p) = .005 in

It should be noted that the laminate properties and processing parameters are required for use with either Equation 3.7 or 3.10 in order to determine the prestrain resulting from the thermal expansion of the filament wound mandrel. This strain, along with the known and derived fiber and matrix properties, is then used in order that Equations 3.45, 3.49, and 3.53 can be simultaneously solved for the unknown coefficients b_0, b_1, and ε_z. Once these coefficients are determined, the stresses in the fiber and matrix can then be determined.

The plots that follow provide the resultant stresses for a variety of levels of prestress, σ_p. With ε_o, the fiber strain caused by the mandrel thermal expansion defined as zero, the resulting stresses are representative of a conventionally cured composite. When a unidirectional laminate is wound and cured, the resulting stress induced into the fibers at the cure temperature is calculated to be approximately 106 ksi. Similarly, the fiber stresses induced through winding-thermal expansion of a crossply laminate are determined to be approximately 112 ksi. The difference between these two methods is the winding/expansion process used to fabricate the crossply laminates produces a biaxial state

of stress in the mandrel resulting in a higher level of prestress. Higher levels of prestress are possible through the application of an additional mechanical force to the fibers. As shown by Figure 3.3, the most dramatic changes are obtained in the longitudinal matrix stress. Since the ultimate strength of a modern epoxy is approximately 12 ksi, the longitudinal matrix stress in a conventionally cured composite is over 40% of the ultimate strength of the neat resin.

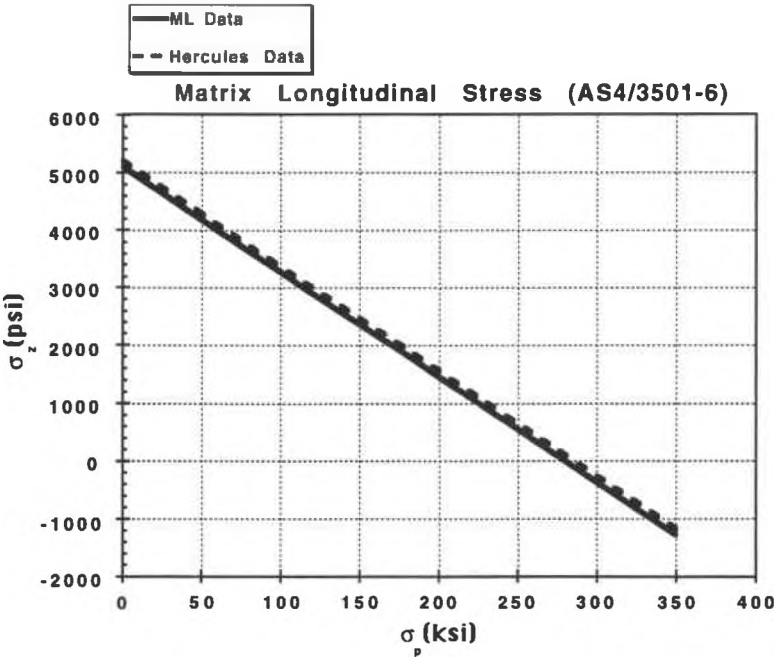

Figure 3.3 Matrix Longitudinal Stress (AS-4/3501-6)

The prestress induced into the fibers as a result of filament winding and thermal expansion alone yields approximately a 38% reduction in the matrix longitudinal stress for the case of a unidirectional composite or an approximate 39% decrease for a crossply laminate. When the applied prestress is greater than 275 ksi, the matrix is actually forced into compression. Modification of the matrix longitudinal stress has been shown to be a major result of the prestress process. Figure 3.4 shows that the fiber longitudinal stress also shows

considerable change. Relative to the strength of the fibers, this change is small so that it is possible that modifying this stress will have little effect on improving or degrading overall composite response. However, since the fibers can reach a point where they are held under tension during the cure cycle, modification of this stress could lead to improved fiber alignment.

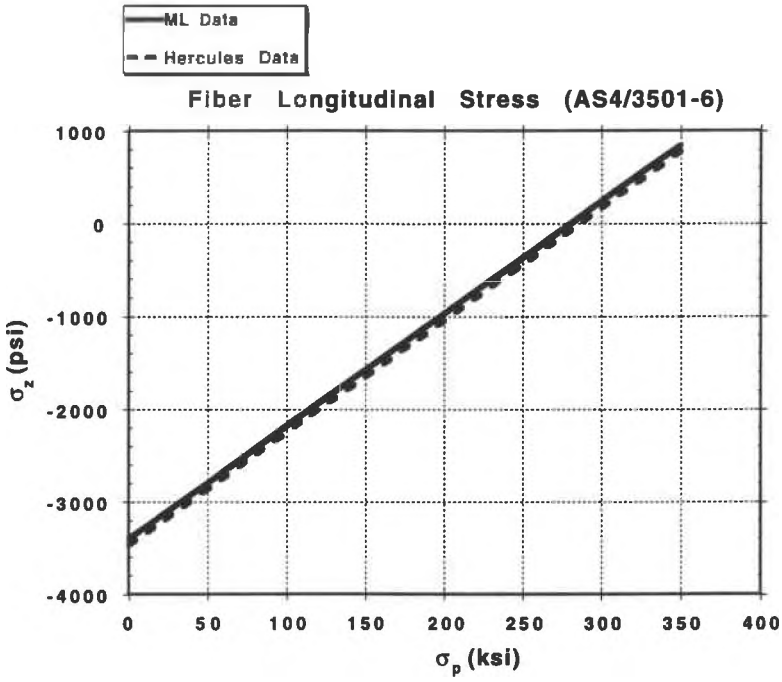

Figure 3.4 Fiber Longitudinal Stress (AS-4/3501-6)

It is obvious that the stresses shown in Figures 3.3 and 3.4 are insensitive to changes in the fiber transverse CTE since the "ML" and "Hercules" curves nearly coincide. This is due to the predominant factor determining these stresses being the longitudinal force balance between the fiber and matrix. This force balance is dependent on the constituent material properties and in the longitudinal direction, the fiber longitudinal modulus is the dominant term. Another factor minimizing the transverse CTE is the fact that its contribution to the longitudinal force balance is reduced due to poissons effect. Analysis of the radial and hoop stresses shows that prestressing also has little influence in modifying

these stresses. The hoop stresses at both the interface between the fiber and matrix as well as the outer matrix cylinder radius are plotted in Figures 3.5 and 3.6.

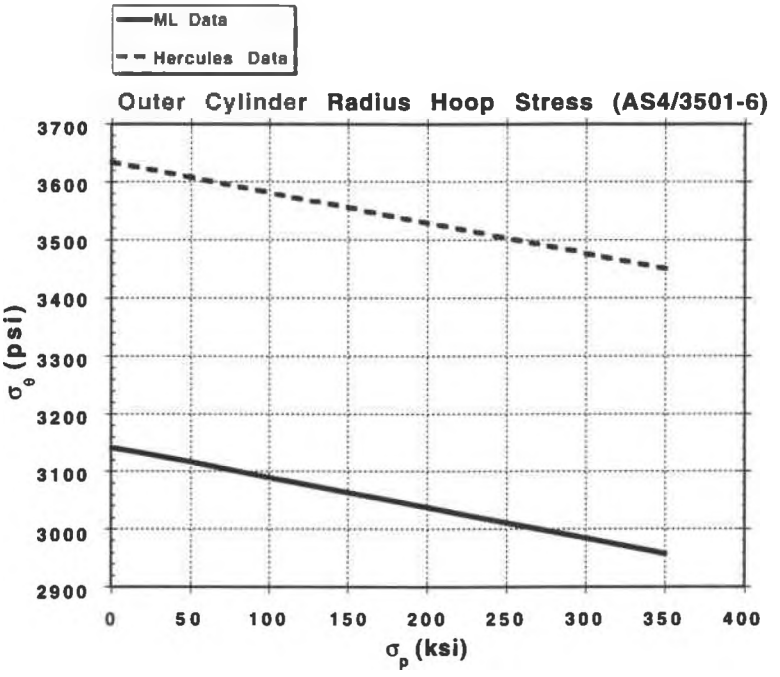

Figure 3.5 Matrix Circumferential Stress at Cylinder Outer Radius (AS-4/3501-6)

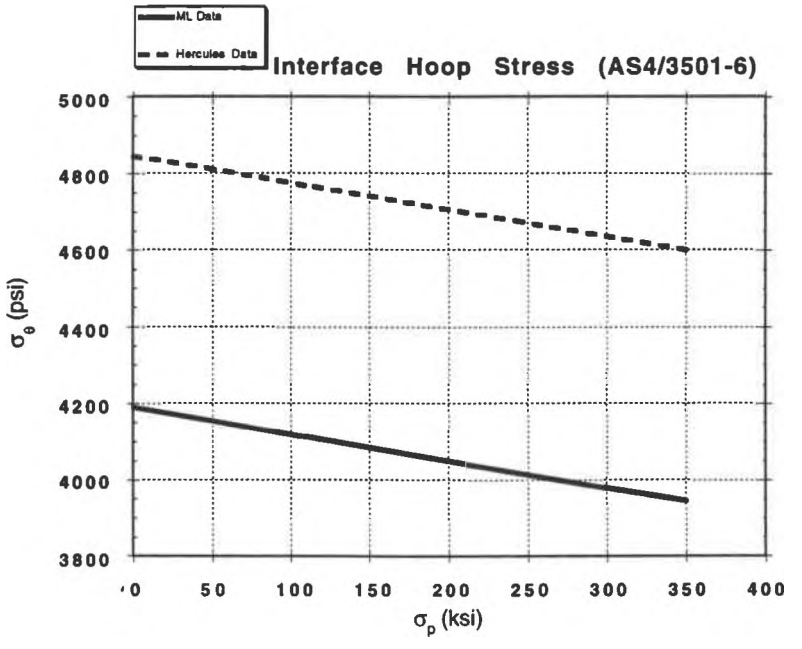

Figure 3.6 Matrix Circumferential Stress at Fiber/Matrix Interface (AS-4/3501-6)

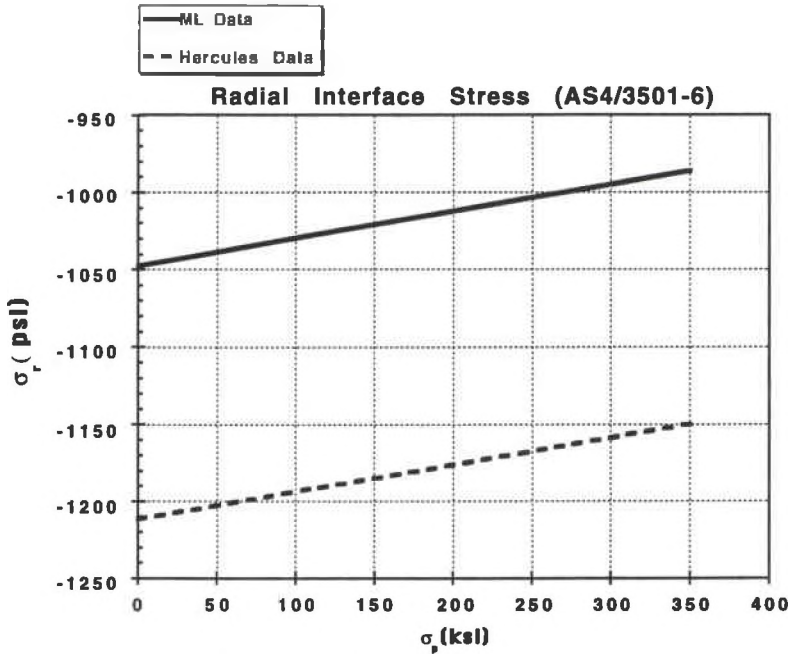

Figure 3.7 Radial Stress at Fiber/Matrix Interface (AS-4/3501-6)

Inspection of these two plots reveals that these stresses vary little with increasing fiber prestress. However, they are more sensitive to changes in the fiber transverse CTE than the longitudinal stresses discussed previously. This should not be surprising since the parametric analysis previously conducted evaluated the hoop strain at the outer cylinder radius as a function of fiber transverse CTE. The radial stress at the fiber/matrix interface also has a slight reduction in the overall magnitude with increasing prestress (see Figure 3.7). Like the hoop stresses, the change is small compared to the magnitude of the applied stress. For both the hoop and radial stresses, a fiber prestress of 350 ksi yields less than a 6% reduction in the magnitude of these stresses.

Analysis of the stresses determined by the model indicates that some of the stresses are vastly altered while others show less change. The obvious benefit of applying a prestress to fibers is the reduction in the matrix longitudinal stresses. It should be noted that the

selection of a 350 ksi maximum prestress was not entirely arbitrary. This level was selected since it represented approximately 70% of the ultimate strength of AS-4 fibers, the same as those used for the experimental measurements. It was felt that applying a load greater than this would risk damaging the fibers during the fabrication process.

6. ANALYTICAL RESULTS FOR THE NICALON/1723 GLASS SYSTEM:

Since it was evident that prestressing reduced the residual stresses in the AS-4/3501-6 graphite/epoxy system, it was felt that there could be an even larger reduction in a system that had both a stiffer matrix as well as a larger ΔT. A great deal of research has recently been conducted in ceramic and glass ceramic composites for high temperature applications. A major obstacle for further development of these materials is the tendency for them to undergo microcracking during cool-down due to the mismatch in CTE's. Due to this problem, a prestress analysis was conducted in order to determine if the stresses causing the microcracking could be reduced sufficiently in order to preclude the cracking. For this analysis, Nicalon fibers and a 1723 glass matrix were chosen. The properties shown below are representative of these materials.

Fiber: $E_1^f = E_2^f = 29.0 \times 10^6$ psi $\quad \nu_{12}^f = \nu_{23}^f = 0.3$

$\alpha_1^f = \alpha_2^f = 2.33 \times 10^{-6}$ in/in (Isotropic Properties)

Matrix: $E^m = 12.76 \times 10^6$ psi $\quad \nu^m = 0.31 \quad \alpha^m = 2.89 \times 10^{-6}$ in/in

Processing: $V_f = 0.4 \quad \Delta T_1 = 1762^oF \quad \Delta T_2 = -1762^oF$

The radial and matrix hoop stresses are shown in Figures 3.8 and 3.9. It is apparent that as was shown for the case of the organic matrix composite, these stresses change. However, the degree of the change is small in comparison to the applied stress.

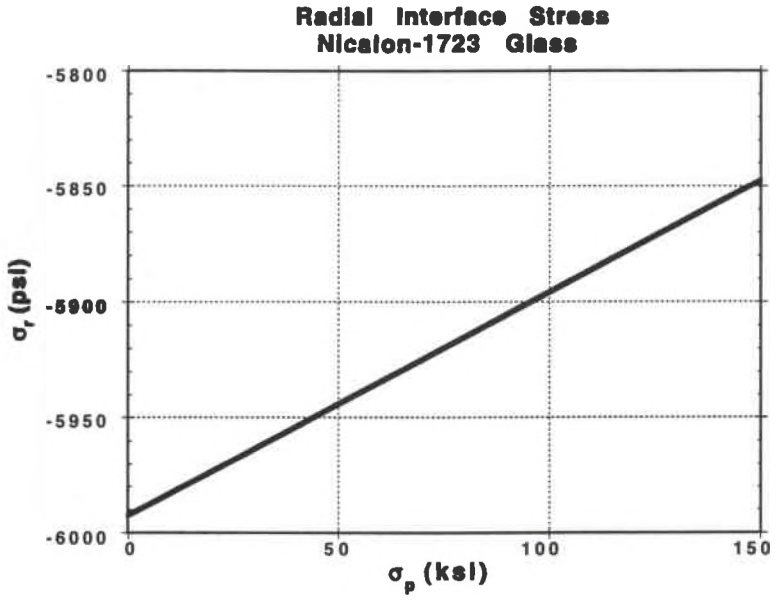

Figure 3.8 Radial Stress at Fiber/Matrix Interface (Nicalon/1723 glass)

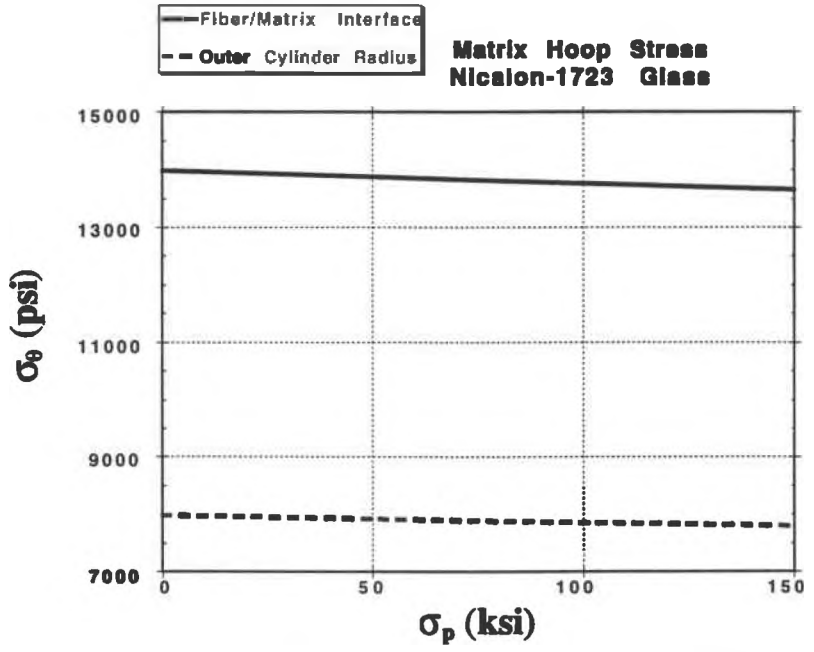

Figure 3.9 Matrix Circumferential Stress (Nicalon/1723 glass)

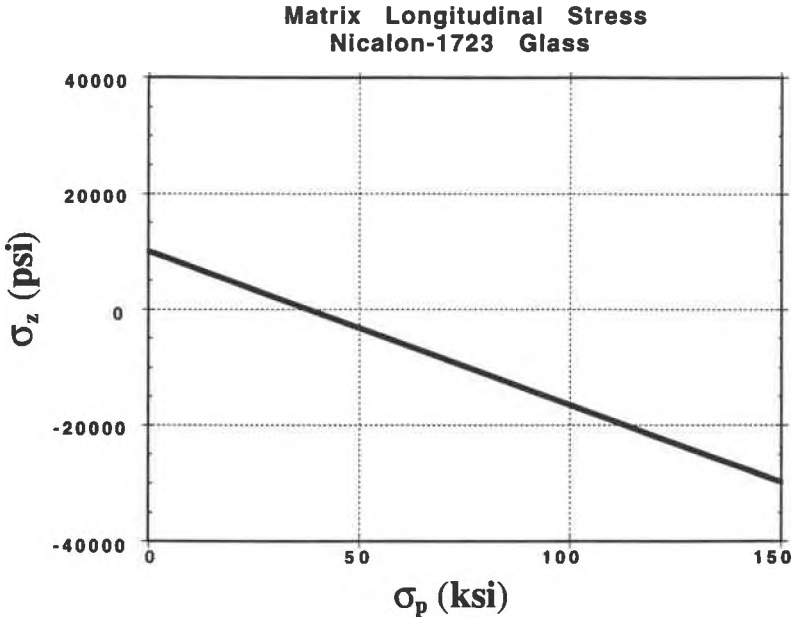

Figure 3.10 Matrix Longitudinal Stress (Nicalon/1723 glass)

Figure 3.10 shows the relationship between the matrix longitudinal stress and the applied prestress. As was evident previously, this stress dramatically changes with increasing prestress. However, a major difference in this case in that the stress is modified much more quickly. This is due to the stiffer matrix material typically seen in ceramic composites. Any equilibrium strain modification has the tremendous ability to be immediately translated into large changes in stress as a result of the force balance existing longitudinally between the fibers and matrix. In the case of the organic matrix composite, the low matrix stiffness meant that the matrix could undergo a considerable amount of elastic strain with little change in its stress.

Figure 3.11 shows how the fiber longitudinal stress is modified by increasing the prestress. The magnitude of this change is large in comparison to that observed in the AS-4 fibers previously analyzed. However, the maximum stress, 40 ksi at a prestress of 150 ksi, is relatively small in comparison to the ultimate strength of the fibers. Since the purpose of

fibers in a ceramic composite is to increase the toughness, it was felt that the increase in fiber stress was not detrimental to the composite performance.

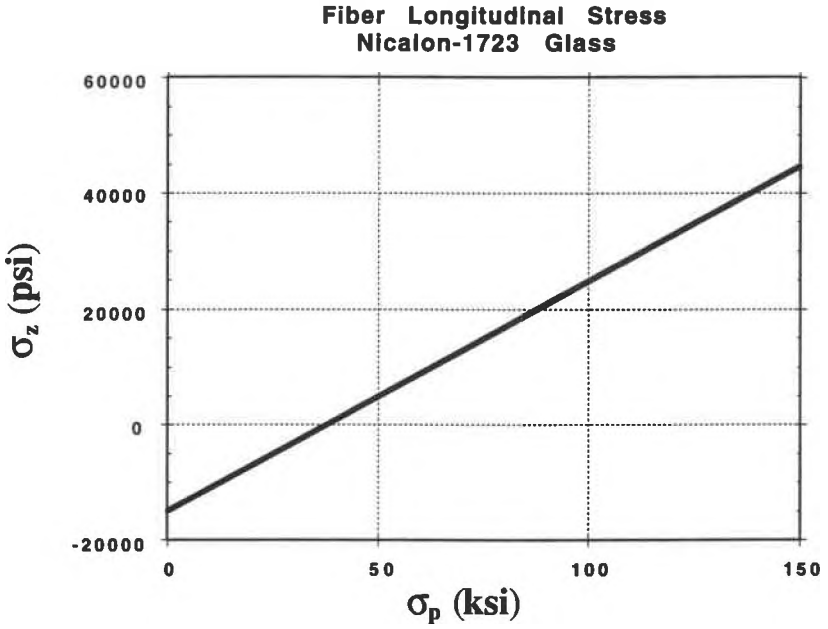

Figure 3.11 Fiber Longitudinal Stress (Nicalon/1723 glass)

CHAPTER IV

LAMINATE ANALYSIS

1. Modification of Classical Laminated Plate Theory: The preceding analysis was important because it predicts the behavior of a unidirectional lamina under uniaxial tension. However, most composites consist of orthotropic plies which are oriented at angles with respect to each other. The ply angular mismatch and their orthotropic behavior result in material properties which vary from ply to ply with respect to the global coordinate system. This variation along with a prescribed laminate loading induces a complex state of stress within the plies which cannot be predicted by the composite cylinders model alone. In order to determine these stresses, a laminate analysis including the strains attributed to the application of a prestress is required. The following is a modification of the laminate analysis previously presented by Jones [8]. This modification allows for the accurate prediction of the in-plane stresses which are dependent on the fiber prestress.

The classical thermomechanical constitutive relations for the k^{th} ply in a laminate are given as

$$\begin{bmatrix} \sigma_x \\ \sigma_y \\ \tau_{xy} \end{bmatrix}_k = \begin{bmatrix} Q_{11} & Q_{12} & Q_{16} \\ Q_{12} & Q_{22} & Q_{26} \\ Q_{16} & Q_{26} & Q_{66} \end{bmatrix}_k \begin{bmatrix} \varepsilon_x - \alpha_x \Delta T \\ \varepsilon_y - \alpha_y \Delta T \\ \gamma_{xy} - \alpha_{xy} \Delta T \end{bmatrix}_k \tag{4.1}$$

in which x and y refer to the coordinate system aligned with the global axes of the plate. In order to easily describe the concentric cylinder model, the cylindrical coordinate system

was used. However, using the associated notation for the laminate analysis would be cumbersome. Therefore, the notation will be changed so that the z,r,θ cylindrical coordinates previously used will be renamed as 1,2,3 coordinates for description of the principle material directions.

The thermal equilibrium strains, including the "preload" effects, obtained as a result of the concentric cylinder model are assumed to be equal to the lamina thermal strains. In order to proceed with the laminate calculations, these strains must be transformed to derive the laminae thermal strains which are functions of the various ply angular orientations with respect to the x-y global coordinates. Equations 4.2 are the relationships required to transform these strains.

$$\begin{bmatrix} \varepsilon_x^T \\ \varepsilon_y^T \\ \gamma_{xy}^T \end{bmatrix}_k = \begin{bmatrix} \cos^2\phi & \sin^2\phi \\ \sin^2\phi & \cos^2\phi \\ 2\sin\phi\cos\phi & -2\sin\phi\cos\phi \end{bmatrix}_k \begin{bmatrix} \varepsilon_1^T \\ \varepsilon_2^T \\ 0 \end{bmatrix} \tag{4.2}$$

where ε_x^T, ε_y^T, and γ_{xy}^T are the ply dependent transformed lamina thermal strains, including the effects of the prestressed fibers and ϕ is the fiber angle of the k^{th} ply.

The classical relations (4.1) must be modified to reflect the prestress dependent thermal strains. The first of these strains, the equilibrium longitudinal preload strain, ε_1^T ($=\varepsilon_z$), is obtained directly from the composite cylinders model and is assumed to be equivalent to the lamina thermal strain in the fiber direction. The equilibrium transverse preload strain, ε_2^T, is not obtained directly from the cylinder model. However, it can be determined by analyzing the cylinder model radial displacement at the juncture between the matrix and the bulk composite (R = 1.0). Due to symmetry, the radial displacement determined through Equations 3.22 and 3.39 is independent of specific radial direction. Therefore, obtaining the average transverse preload strain is a simple matter of evaluating the radial displacement

at the outer matrix radius and dividing by that radius. This strain is observed to be equivalent to the cylinder hoop strain, Equation 3.40 evaluated at the matrix outer radius.

$$\varepsilon_2^T = b_0 + \frac{b_1}{1^2} = b_0 + b_1 \ (= \varepsilon_\theta) \tag{4.3}$$

Equations 4.2 and 4.3 along with the equilibrium longitudinal preload strain are now applied to modify Equations 4.1 resulting in constitutive equations which include the effects of thermal processing and fiber prestress

$$\begin{bmatrix} \sigma_x \\ \sigma_y \\ \tau_{xy} \end{bmatrix}_k = \begin{bmatrix} Q_{11} & Q_{12} & Q_{16} \\ Q_{12} & Q_{22} & Q_{26} \\ Q_{16} & Q_{26} & Q_{66} \end{bmatrix}_k \begin{bmatrix} \varepsilon_x - \varepsilon_x^T \\ \varepsilon_y - \varepsilon_y^T \\ \gamma_{xy} - \gamma_{xy}^T \end{bmatrix}_k \tag{4.4}$$

where ε_x, ε_y, and γ_{xy} are the applied strains due to loading.

The applied strains ε_x, ε_y, and γ_{xy} can be replaced by the following expression

$$\begin{bmatrix} \varepsilon_x \\ \varepsilon_y \\ \gamma_{xy} \end{bmatrix} = \begin{bmatrix} \varepsilon_x^o \\ \varepsilon_y^o \\ \gamma_{xy}^o \end{bmatrix} + z \begin{bmatrix} k_x \\ k_y \\ k_{xy} \end{bmatrix} \tag{4.5}$$

where ε_x^o, ε_y^o, and ε_{xy}^o are the midplane strains, z is the distance from the laminate midplane and the k's represent the midplane curvatures. The solution of Equations 4.5 requires that the midplane strains and curvatures be known. These can be determined through knowledge of the material properties, laminate geometry, and applied loading, including the effect of fiber prestressing. The resultant force matrix is determined by

$$\begin{bmatrix} \overline{N_x} \\ \overline{N_y} \\ \overline{N_{xy}} \end{bmatrix} = \begin{bmatrix} N_x + N_x^T \\ N_y + N_y^T \\ N_{xy} + N_{xy}^T \end{bmatrix} = \begin{bmatrix} A_{11} & A_{12} & A_{16} \\ A_{12} & A_{22} & A_{26} \\ A_{16} & A_{26} & A_{66} \end{bmatrix} \begin{bmatrix} \varepsilon_x^o \\ \varepsilon_y^o \\ \gamma_{xy}^o \end{bmatrix} + \begin{bmatrix} B_{11} & B_{12} & B_{16} \\ B_{12} & B_{22} & B_{26} \\ B_{16} & B_{26} & B_{66} \end{bmatrix} \begin{bmatrix} k_x \\ k_y \\ k_{xy} \end{bmatrix} \tag{4.6}$$

Where the fictitious forces due to the application of the prestress are defined as

$$\begin{bmatrix} N_x^T \\ N_y^T \\ N_{xy}^T \end{bmatrix} = \int \begin{bmatrix} Q_{11} & Q_{12} & Q_{16} \\ Q_{12} & Q_{22} & Q_{26} \\ Q_{16} & Q_{26} & Q_{66} \end{bmatrix}_k \begin{bmatrix} \varepsilon_x^T \\ \varepsilon_y^T \\ \gamma_{xy}^T \end{bmatrix}_k dz \tag{4.7}$$

The resultant moment matrix is of similar form.

$$\begin{bmatrix} \overline{M_x} \\ \overline{M_y} \\ \overline{M_{xy}} \end{bmatrix} = \begin{bmatrix} M_x + M_x^T \\ M_y + M_y^T \\ M_{xy} + M_{xy}^T \end{bmatrix} = \begin{bmatrix} B_{11} & B_{12} & B_{16} \\ B_{12} & B_{22} & B_{26} \\ B_{16} & B_{26} & B_{66} \end{bmatrix} \begin{bmatrix} \varepsilon_x^o \\ \varepsilon_y^o \\ \gamma_{xy}^o \end{bmatrix} + \begin{bmatrix} D_{11} & D_{12} & D_{16} \\ D_{12} & D_{22} & D_{26} \\ D_{16} & D_{26} & D_{66} \end{bmatrix} \begin{bmatrix} k_x \\ k_y \\ k_{xy} \end{bmatrix} \tag{4.8}$$

Where the fictitious moments due to the application of the prestress are defined as

$$\begin{bmatrix} M_x^T \\ M_y^T \\ M_{xy}^T \end{bmatrix} = \int \begin{bmatrix} Q_{11} & Q_{12} & Q_{16} \\ Q_{12} & Q_{22} & Q_{26} \\ Q_{16} & Q_{26} & Q_{66} \end{bmatrix}_k \begin{bmatrix} \varepsilon_x^T \\ \varepsilon_y^T \\ \gamma_{xy}^T \end{bmatrix}_k zdz \tag{4.9}$$

Equations 4.6 and 4.8 can be rewritten in the following matrix form

$$\begin{bmatrix} \overline{N} \\ \overline{M} \end{bmatrix} = \begin{bmatrix} A & B \\ B & D \end{bmatrix} \begin{bmatrix} \varepsilon^o \\ k \end{bmatrix} \tag{4.10}$$

Inversion of Equation 4.10 yields a relation for determining the midplane strains and curvatures in terms of the applied resultant forces and moments.

$$\begin{bmatrix} \varepsilon^o \\ k \end{bmatrix} = \begin{bmatrix} A^* B^* \\ B^* D^* \end{bmatrix} \begin{bmatrix} \overline{N} \\ \overline{M} \end{bmatrix} \tag{4.11}$$

The solution for the ply stresses are obtained by evaluating Equations 4.11, using the results to determine the z dependent strains from Equations 4.5 and finally determining the ply stresses using Equation 4.4.

2. DETERMINATION OF THE LAMINA EFFECTIVE COEFFICIENTS OF THERMAL EXPANSION: Consider the AS-4/3501-6 unidirectional lamina properties .

$E_1 = 20 \times 10^6$ psi $\quad E_2 = 1.5 \times 10^6$ psi $\quad G_{12} = 0.8 \times 10^6$ psi $\quad \nu_{12} = 0.3$
$X_t = X_c = 300$ ksi $\quad Y_t = 7.5$ ksi $\quad Y_c = 30$ ksi $\quad S = 13.5$ ksi

For use in the following laminate analysis, the thermal strains typically determined through $\alpha\Delta T$ calculations will be replaced with the thermal equilibrium strains calculated by the concentric cylinder model. Tables 4.1 and 4.2 contain these strains. As mentioned before, two solutions for the equilibrium strains will be used in order to bound the solution.

Table 4.1
Strains Obtained from the Concentric Cylinder Model (Hercules Data)

σ_p (ksi)	ε_1^T (in/in)	ε_2^T (in/in)
0	9.5020×10^{-6}	-3.3740×10^{-3}
50	-1.4430×10^{-3}	-2.9170×10^{-3}
106	-3.0950×10^{-3}	-2.3990×10^{-3}
112	-3.2420×10^{-3}	-2.3530×10^{-3}
150	-4.3490×10^{-3}	-2.0050×10^{-3}
200	-5.8020×10^{-3}	-1.5490×10^{-3}
250	-7.2550×10^{-3}	-1.0920×10^{-3}
300	-8.7080×10^{-3}	-6.3580×10^{-4}
350	-1.0160×10^{-2}	-1.7930×10^{-4}

Table 4.2
Strains Obtained from the Concentric Cylinder Model (ML Data)

σ_p (ksi)	ε_1^T (in/in)	ε_2^T (in/in)
0	-1.0960×10^{-4}	-4.1200×10^{-3}
50	-1.3430×10^{-3}	-3.6540×10^{-3}
106	-2.9820×10^{-3}	-3.1390×10^{-3}
112	-3.1330×10^{-3}	-3.0910×10^{-3}
150	-4.2490×10^{-3}	-2.7410×10^{-3}
200	-5.7020×10^{-3}	-2.2840×10^{-3}
250	-7.1550×10^{-3}	-1.8280×10^{-3}
300	-8.6080×10^{-3}	-1.3710×10^{-3}
350	-1.0060×10^{-2}	-9.1490×10^{-4}

Since the strains contained in Tables 4.1 and 4.2 are functions of temperature, they can be used to introduce the concept of the effective thermal expansion coefficient. Essentially what occurs as a result of prestressing is that the expansional strains due to processing contain two components: one from the actual mismatch in constituent CTE's and the other from the application of a load to the fibers during the cure cycle. Following cure, the contribution of the fiber prestress to the total expansional strain will be a linearly temperature dependent strain. Since the other portion of the expansional strain, $\alpha\Delta T$, can also be considered to be linearly temperature dependent, the combination of both terms can be thought of as the result of an effective CTE. The strains listed in Tables 4.1 and 4.2 are a result of the superposition of the two strain components. In order to determine the effective CTE, the strains must simply be divided by the change from the cure to the use temperature, ΔT_2.

$$\overline{\alpha_1} = \frac{\varepsilon_1^T}{\Delta T_2} \qquad \overline{\alpha_2} = \frac{\varepsilon_2^T}{\Delta T_2} \tag{4.12}$$

Table 4.3
Effective Thermal Expansion Coefficients (Hercules Data)

σ_p (ksi)	$\overline{\alpha}_1$ (in/in °F)	$\overline{\alpha}_2$ (in/in °F)
0	-3.3936×10^{-8}	1.2050×10^{-5}
50	5.1536×10^{-6}	1.0418×10^{-5}
106	1.1054×10^{-5}	8.5679×10^{-6}
112	1.1579×10^{-5}	8.4036×10^{-6}
150	1.5532×10^{-5}	7.1607×10^{-6}
200	2.0721×10^{-5}	5.5321×10^{-6}
250	2.5911×10^{-5}	3.9000×10^{-6}
300	3.1100×10^{-5}	2.2707×10^{-6}
350	3.6286×10^{-5}	6.4036×10^{-7}

Table 4.4
Effective Thermal Expansion Coefficients (ML Data)

σ_p (ksi)	$\overline{\alpha}_1$ (in/in °F)	$\overline{\alpha}_2$ (in/in °F)
0	3.9143×10^{-7}	1.4714×10^{-5}
50	4.7964×10^{-6}	1.3050×10^{-5}
106	1.0650×10^{-5}	1.1211×10^{-5}
112	1.1189×10^{-5}	1.1039×10^{-5}
150	1.5175×10^{-5}	9.7893×10^{-6}
200	2.0364×10^{-5}	8.1571×10^{-6}
250	2.5554×10^{-5}	6.5286×10^{-6}
300	3.0743×10^{-5}	4.8964×10^{-6}
350	3.5929×10^{-5}	3.2675×10^{-6}

Since the laminate analysis about to be accomplished requires longitudinal and transverse properties, the appropriate subscripts are used. Equations 4.12 are used to determine the effective CTE's. Tables 4.3 and 4.4 contain the appropriate data which was obtained by using these two equations in conjunction with the previously derived strains.

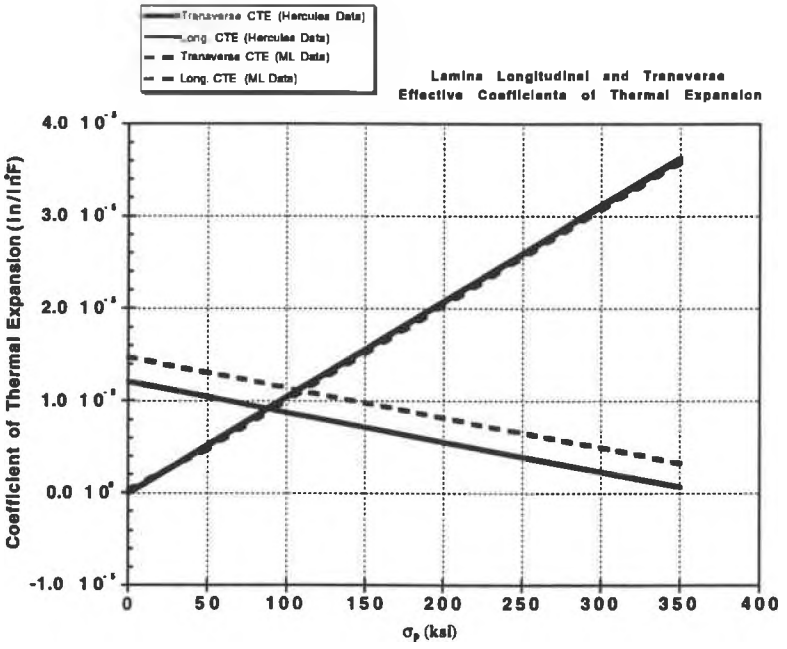

Figure 4.1 The Variance of Thermal Expansion Coefficients as a Function of Prestress

Figure 4.1 graphically depicts the data contained in Tables 4.3 and 4.4. The interesting thing to note is that the curves intersect at a prestress of approximately 100 ksi, thus indicating a thermally isotropic material at this point. Coincidentally, the intersection occurs at a level of prestress which is close to the level predicted for the case of a unidirectional laminate used in the experimental portion of this research.

3. GENERALIZATION OF LAMINATE EQUATIONS FOR CROSSPLY LAMINATES:

For the case of a crossply laminate with applied extensional forces, Equations 4.4 can be significantly reduced since all moments, shear strains, midplane curvatures, and the

reduced stiffnesses $Q_{16}^{(k)}$ and $Q_{26}^{(k)}$ equal zero. The constitutive equations for this case are

$$\begin{bmatrix} \sigma_x \\ \sigma_y \\ \tau_{xy} \end{bmatrix}_k = \begin{bmatrix} Q_{11} & Q_{12} & 0 \\ Q_{12} & Q_{22} & 0 \\ 0 & 0 & Q_{66} \end{bmatrix}_k \begin{bmatrix} \varepsilon_x - \varepsilon_x^T \\ \varepsilon_y - \varepsilon_y^T \\ \gamma_{xy} \end{bmatrix}_k \tag{4.13}$$

where the applied strains ε_x, ε_y, and γ_{xy} are equal to the midplane strains. The strain components, $\varepsilon_x{}^T$ and $\varepsilon_y{}^T$, are the environmental strains due to the application of the thermally dependent prestress. These strains are ply dependent and are obtained by obtaining data from Tables 4.1 and 4.2 and transforming using Equations 4.2 and 4.12.

$$\begin{array}{lll} \text{1st and 4th plies} & \varepsilon_x^T = \overline{\alpha_1}\Delta T_2 & \varepsilon_y^T = \overline{\alpha_2}\Delta T_2 \\ \text{2nd and 3rd plies} & \varepsilon_x^T = \overline{\alpha_2}\Delta T_2 & \varepsilon_y^T = \overline{\alpha_1}\Delta T_2 \end{array} \tag{4.14}$$

Since N_{xy}^T and the midplane curvatures equal zero, Equations 4.6 can be rewritten in order to solve for the midplane strains

$$\begin{bmatrix} \varepsilon_x^o \\ \varepsilon_y^o \\ \gamma_{xy}^o \end{bmatrix} = \begin{bmatrix} A'_{11} & A'_{12} & 0 \\ A'_{12} & A'_{22} & 0 \\ 0 & 0 & A'_{66} \end{bmatrix} \begin{bmatrix} N_x + N_x^T \\ N_y + N_y^T \\ N_{xy} \end{bmatrix} \tag{4.15}$$

where the fictitious prestress forces are given by Equations 4.7. Substituting 4.15 into 4.13 and expanding yields the ply stresses

$$\begin{aligned} \sigma_x^{(k)} = {} & Q_{11}^{(k)}\left[A'_{11}\left(N_x + N_x^T\right) + A'_{12}\left(N_y + N_y^T\right) - \varepsilon_x^{T\,(k)}\right] \\ & + Q_{12}^{(k)}\left[A'_{12}\left(N_x + N_x^T\right) + A'_{22}\left(N_y + N_y^T\right) - \varepsilon_y^{T\,(k)}\right] \end{aligned} \tag{4.16}$$

$$\begin{aligned} \sigma_y^{(k)} = {} & Q_{12}^{(k)}\left[A'_{11}\left(N_x + N_x^T\right) + A'_{12}\left(N_y + N_y^T\right) - \varepsilon_x^{T\,(k)}\right] \\ & + Q_{22}^{(k)}\left[A'_{12}\left(N_x + N_x^T\right) + A'_{22}\left(N_y + N_y^T\right) - \varepsilon_y^{T\,(k)}\right] \end{aligned} \tag{4.17}$$

$$\tau_{xy}^{(k)} = Q_{66}^{(k)} A'_{11} N_{xy} \tag{4.18}$$

Since the strains that result from the application of a prestress to the fibers are significantly different than those normally seen in conventional laminates, it seems likely that the structural response of these laminates should change. For this reason, use of an appropriate failure criterion with the previously derived constitutive relations is required. The maximum stress criterion provides an easy way to at least establish trends in the changes in laminate structural response as a result of changing prestress levels. Although this analysis may not provide the most accurate prediction for composite failure, the method certainly provides information that will quantify changes in composite strength in response to increasing levels of fiber prestress.

The first layers to fail in a crossply (4 layer) laminate are the inner (90^0) plies. This failure is caused by the stress in the loading direction exceeding the lamina transverse tensile strength. To solve for the load required to cause first ply failure, the lamina transverse tensile strength and the second ply material properties were substituted into Equation 4.16 and the resulting expression was rewritten to solve for the maximum applied unidirectional load, N_x/t where t is the laminate thickness. Figure 4.2 shows the load required to initiate first ply failure as a function of the prestress induced into the fibers. The figure demonstrates that increasing the level of fiber prestress linearly changes the amount of applied load that is required in order to cause first ply failure. Since the first ply failure load shows a dramatic increase with increasing prestress, the strain seen at first ply failure is much larger than those typically seen in conventional laminates (see Figure 4.3).

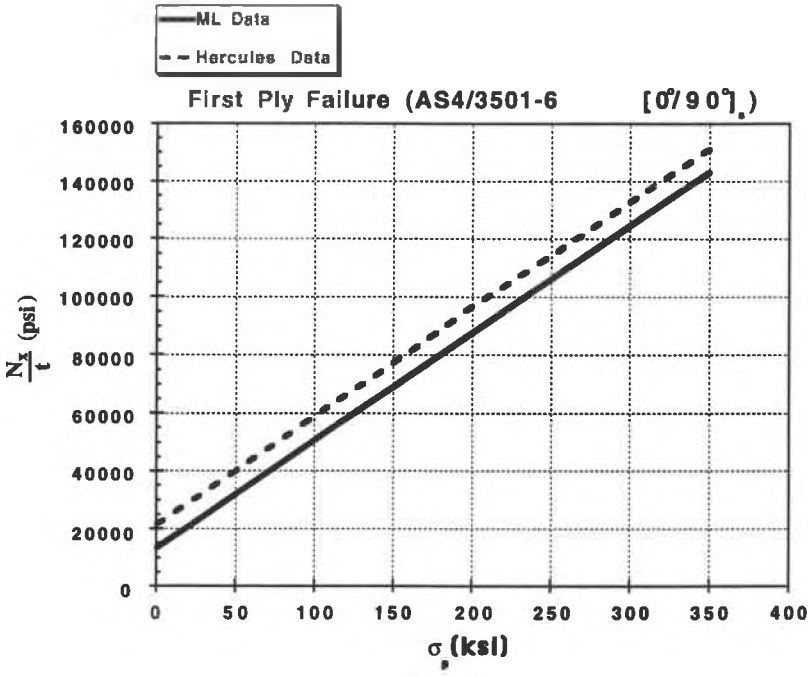

Figure 4.2 Load Required to Initiate First Ply Failure

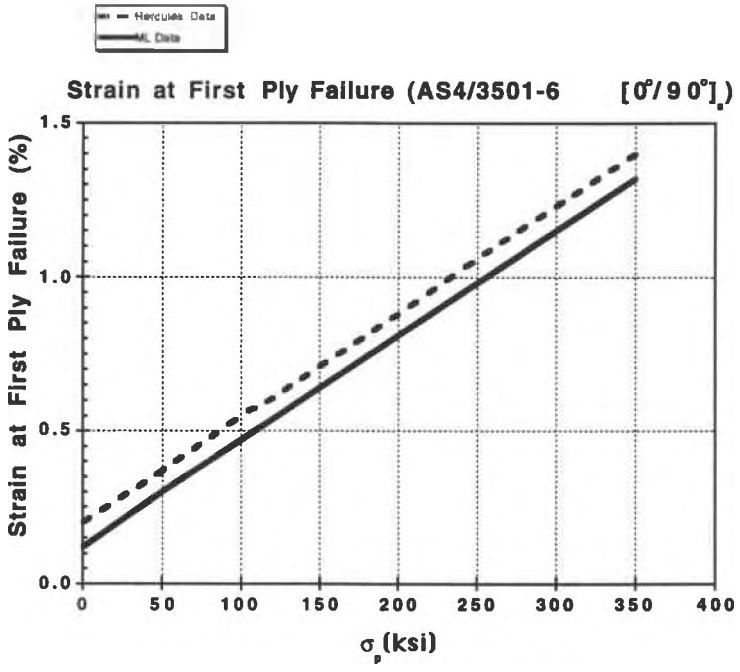

Figure 4.3 Applied Strain at First Ply Failure

CHAPTER V

FABRICATION OF PRESTRESSED LAMINATED PLATES

1. PRESTRESS PROCESSING:

The fabrication of the prestressed laminates requires the application of a mechanical load to the fibers during the cure cycle. The load induced must be of significant magnitude for the desired stress modification but low enough so that the amount of fibers fractured is minimized. In order to apply the stress in the fibers, a technique had to be developed that would be easy to accomplish, reproducible, and feasible. The first method considered was to develop a fixture that would clamp the fibers tightly at the ends and then allow for extensional motion resulting in fiber tension. This method was rejected because it was felt that there would be too great of a statistical variation of induced stresses from one fiber to another and that excessive fiber damage could result. The second technique considered was to use a combination of filament winding and thermal expansion to apply the required force to the fibers. This method was chosen because it seemed to provide a reproducible and accurate means of applying a uniform stress in each of the fibers which were continuously wound around the plate.

The selection of filament winding posed a number of difficulties which had to be resolved. Traditionally, filament winding is used for fabricating cylindrical structures such as pressure vessels and tubes. In the present case, uniaxial testing specimens were required which meant that a flat mandrel was necessary. The reason filament winding of cylindrical structures works so well is that the process has a tendency for the composite to self compact, eliminating the requirement of pressure when curing. However, when

attempting to wind a flat plate, the only portion of the winding that self compacts is the region at the rounded edges. In order to compact the flat portion of the plate, external pressure had to be applied, therefore it necessitated the curing of the composite in an autoclave using a conventional graphite/epoxy cure cycle (100 psi, 350°F) .

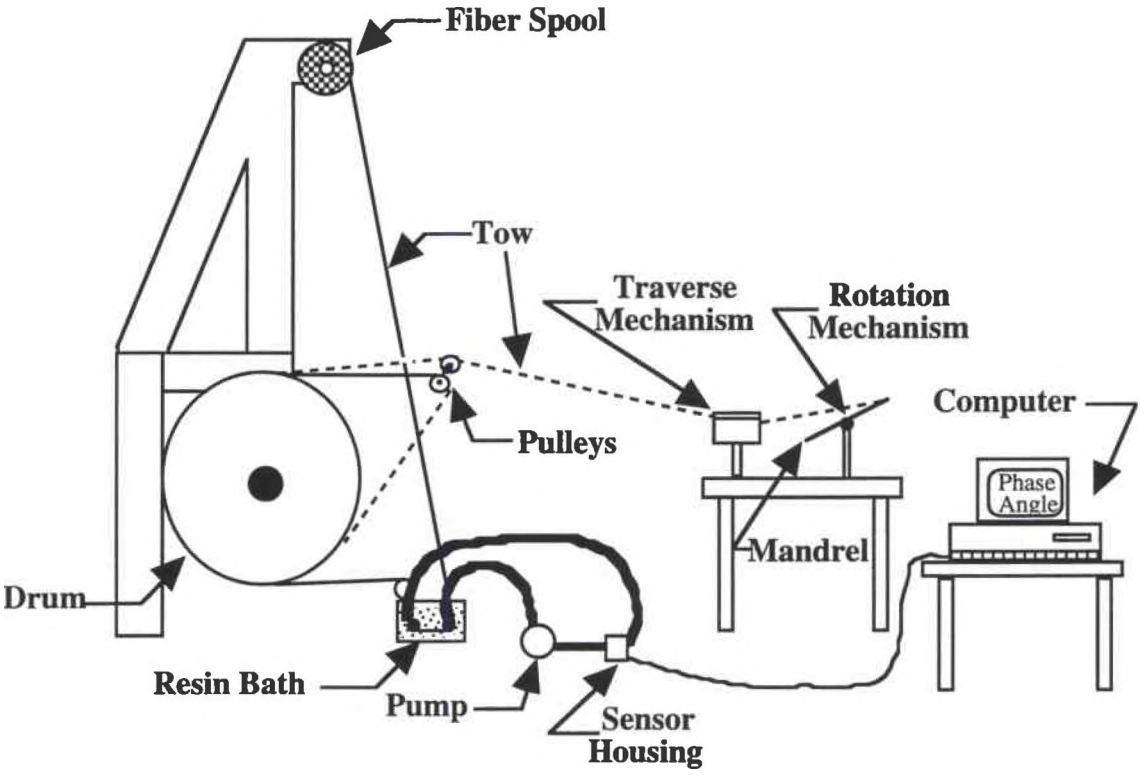

Figure 5.1 Filament Winding Components

Another significant concern was obtaining enough tension in the fiber tow so there would be no slack in the fibers after winding around the mandrel. This was extremely important because the actual extension of the fibers was proportional to the difference in the thermal expansion coefficients of the mandrel and the fibers. If the fibers were not tightly wound around the mandrel, the plate could freely expand with increasing temperature, resulting in no tension being induced into the fibers. In order to ensure the fibers were tightly wound, a tensioning mechanism was constructed by modifying some existing equipment. This equipment included a tabletop filament winder along with a device which is used to make

prepreg. This device includes a large drum and it is this feature which is exploited for the current purpose (see Figure 5.1). The inertia of the drum along with friction caused by a mechanical brake applied to its surface provided the desired tension. The fiber tow was impregnated with resin, wrapped around the surface of the drum, over a pulley, around the drum a second time, over another pulley, and finally into the filament winding equipment. Other details of the process will be discussed later.

2. PROCESS OPTIMIZATION:

Impregnating the fiber tow with resin posed additional challenges. The requirement of high tension in the tow necessitated impregnating the tow with resin prior to inducing the tension. This was required because high tow tension precludes the ability of the liquid resin to migrate to the center of the tow resulting in a composite with resin starved areas and a high fiber volume. Two common means for accomplishing the impregnation are to either use a hot melt procedure where the resin is melted and the tow is passed through pure resin or to solution prepreg where the resin is dissolved in a compatible solvent and the tow is passed through the resulting solution. The hot melt procedure was rejected because the length of travel of the tow following impregnation would allow the resin to cool and the tow to harden. The solution method proved adequate as long as the length of travel after impregnation was kept to a minimum. A shorter travel prevented the solvent from totally evaporating which reduced the tendency of the fibers from sticking to the rollers and pulleys. A number of different mechanical configurations of the filament winding equipment were considered prior to determining an acceptable one.

Choosing the solution method for resin impregnation lead to subsequent problems with high porosity in the laminates. Nondestructive inspections (C-scans) and photomicrographs were used to determine that solvent entrapment was the cause. The technique chosen for eliminating the solvent was to debulk the composite prior to cure

through the use of vacuum and a slightly elevated temperature. This was initially accomplished by vacuum bagging the mandrel/winding and placing the assembly in the autoclave overnight at a temperature of 150^0 F. This procedure was determined to be too complicated as well as an inefficient use of the autoclave. The second method was to simply put the mandrel in a vacuum oven at the same temperature and for the same length of time. This procedure allowed the successful elimination of the solvent which led to good quality laminated plates. However, it was felt that the temperature selected might be causing the resin to partially cure. This led to the final debulk method in which the composite was held under vacuum for 4 hours at 125^0 F. The heating elements were then turned off but the vacuum was again maintained overnight. This method was later validated with successful C-scans and photomicrographs.

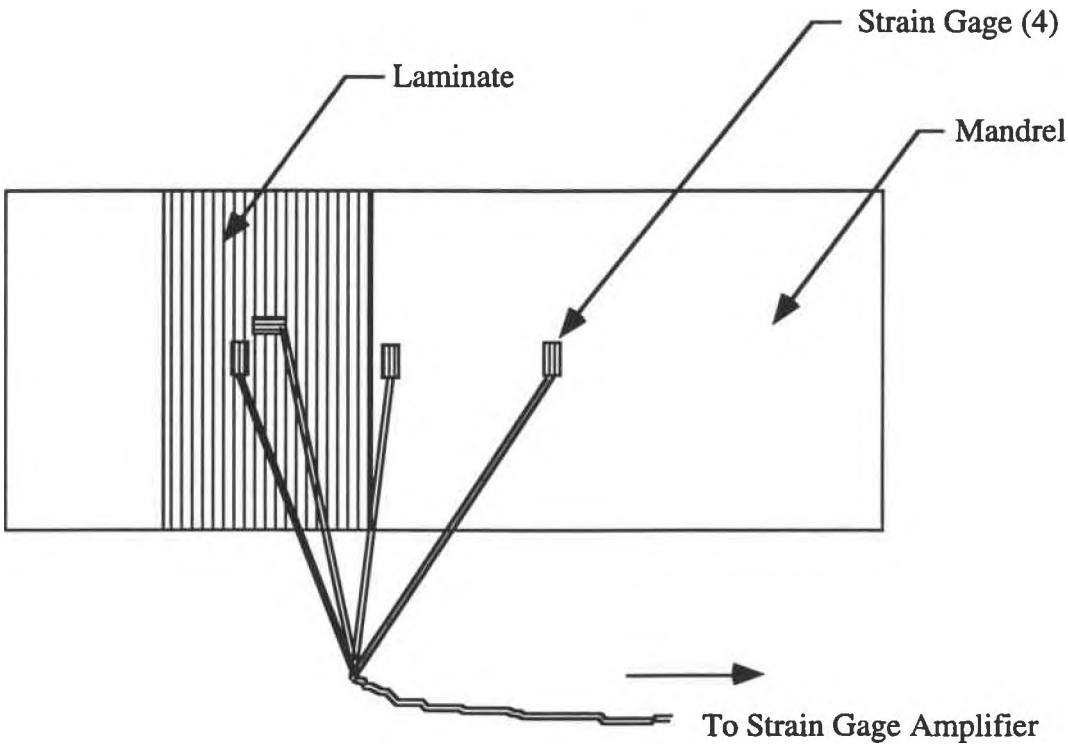

Figure 5.2 Mandrel/Winding Showing Strain Gage Locations

Tests were conducted to determine if the degree of thermal expansion in the laminate during cure was proportional to the expansion of the plate. Strain gages were bonded to the cured laminate while it was still wound around the mandrel. A biaxial rosette was bonded at the middle of the laminate while longitudinal gages were used at two locations on the mandrel (see Figure 5.2). A gage was bonded directly alongside the winding while another was bonded at a distance far removed from the winding. These gages were installed in order to determine whether the winding and mandrel exhibited the same degree of thermal expansion. The mandrel with the continuously wound laminate was then put in an oven and the temperature was raised while output from the various strain gages was obtained. The objective was not to attain data but to ensure the assumption of the fibers and mandrel expanding at the same rate was valid.

The thermal testing revealed that the degree of expansion of the plate and the winding were not identical as predicted. The plate freely expanded up to 160^0 F at which point the laminate and the plate both expanded linearly. The cause of this phenomenon was partly due to the compression of the Teflon®/glass self adhesive release ply bonded to the surface of the mandrel. A further study to determine the degree at which compression of the release ply influenced the expansion of the fibers was conducted. Another plate was wound but in this instance, the peel ply was omitted from the edges of the mandrel. Frekote (a spray release agent) was applied at these points to preclude the laminate from sticking. After winding and cure, the thermal test was repeated but in this case, the mandrel and composite both expanded immediately upon an increase in temperature.

A conventionally cured laminate was also strain gaged and subjected to the same post cure test as above in order to provide a comparison of the prestressed laminate with a conventional laminate. The results indicate that this laminate, unlike the prestressed winding in-situ on the mandrel, did not expand. This is not surprising since the longitudinal CTE in a unidirectional composite is fiber dominated and the fibers have an

extremely low CTE. This test verified that the actual expansion of the winding/mandrel system was due to the interaction of the mandrel and composite and not a fundamental property of the laminate itself.

3. LAMINATE SURFACE FINISH REFINEMENT:

During the learning process required to successfully manufacture the prestressed plates, some problems had to be solved prior to the accomplishment of the mechanical testing. A major problem occurred with the finished surface of the plate. The surface cured adjacent to the mandrel was flat but the opposite side was grooved resulting in a plate with inconsistent thickness. This was attributed to the size of the fiber tow being used. The problem with having an inconsistent thickness was that it was impossible to determine the stress during testing since the cross sectional area of the test coupons could not accurately be measured. In addition, the grooves lead to non-uniform stress fields caused by stress concentrations. A way of minimizing the effect of the fiber tow was to use one with fewer fibers. A 3K tow was obtained to replace the 12K tow previously used. It was felt that reducing the area of the bundle of fibers should make it easier to attain a flatter surface resulting in a plate having a more consistent thickness. However, choosing a tow with significantly fewer fibers was not without its own problems. The tow itself could not withstand much damage before the entire bundle of fibers would fail. The same winding configuration was attempted for the 3K tow as was previously used for the 12K tow. It was known that the harsh requirements of the winding process caused fiber fractures in the 12K tow. These requirements included pulling the tow in a serpentine fashion through a number of pulleys and rollers under a good deal of tension. When the smaller tow was processed in the same fashion, it immediately fractured. A new winding setup was established using Teflon® and Delrin® rollers and pulleys. This new setup satisfactorily eliminated most of the problems that were previously encountered. The surface finish and

thickness of the plate following cure with the new setup were significant improvements over the previous attempts.

Following the establishment of a satisfactory winding method, the determination of winding parameters for use in obtaining reproducible coupon thicknesses had to be established. The winding machine utilized two independently controlled motors for use in both rotating the mandrel as well as controlling the traverse of the fiber tow across the mandrel. In conventional filament winding, a nominal amount of tension is imparted into the tow which allows it to flatten out. However, with the high tow tension required in the current process, the fiber bundle, even after winding, tends to remain circular which degrades the finished surface of the plate. Circular bundles hamper the ability of the tow to overlap one another as the winding continues. To solve this phenomenon, a number of laminates were fabricated using the 3K tow and various winding parameters in order to obtain the optimum thickness testing specimens. The method chosen to determine the proper winding speeds was to initially set the rotation speeds at a rate which seemed to be adequate. This choice was totally subjective but was later validated with analysis of completed panels. After the rotation speed was selected, a number of different panels were wound using various traverse speeds and layers. The thicknesses of these panels after they were cured were then used for extrapolating the final winding parameters. This procedure along with the previously discussed change from the 12K to the 3K tow ultimately led to fabrication of plates that had consistent thickness.

4. PROCESS MONITORING:

The final problem to solve was the high fiber volumes found in the composites. Eliminating this condition proved to be the most difficult portion of the research. It seemed apparent that the problem could be partially attributed to the winding solution being too dilute. It was hoped a larger percentage of epoxy solids could simply be added to the

solution, thus achieving lower fiber volumes in the finished composites. However, starting with a more concentrated solution of acetone/epoxy, as well as increasing the winding times with the change to a 3K tow, allowed what little solvent was left in solution to evaporate. The result was that the entire winding mechanism became sticky with resin causing the tow to fracture. There was also a problem with maintaining control over the solution viscosity. As the winding process progressed, it could be seen that some areas of the plate looked wetter than others. This was due to changes in solution viscosity caused by the periodic addition of solvent into the resin bath.

In order to minimize the changes in the solution viscosity, it was felt some sort of process monitoring could be used as a tool for adding solvent. The additional solvent, if added in correct quantities, would maintain an optimum resin content in the solution. A Micromet Eumetric System II Microdielectrometer along with an Idex sensor was used to make a series of dielectric measurements on various concentrations of the epoxy/acetone solutions. The hope was that by varying the concentrations of the solutions, some electrical characteristic of the solution would change. This change would allow for the monitoring and control of the solution concentration during the winding process. The results from these tests indicated the phase angle varied as a function of the viscosity (See Figure 5.3). The interesting thing to note is that a cubic curve fit well through the data points and that the slope of the curve changed rapidly after the concentration of the solution reached approximately 55% solids. In an actual winding environment, the smallest percentage of solids present would be 50% (the starting concentration). Since evaporation of the solvent would increase the concentration above 55%, monitoring the phase angle of the solution and adding solvent as necessary appears to be a valid means of controlling viscosity and ultimately, the fiber volume of the laminate.

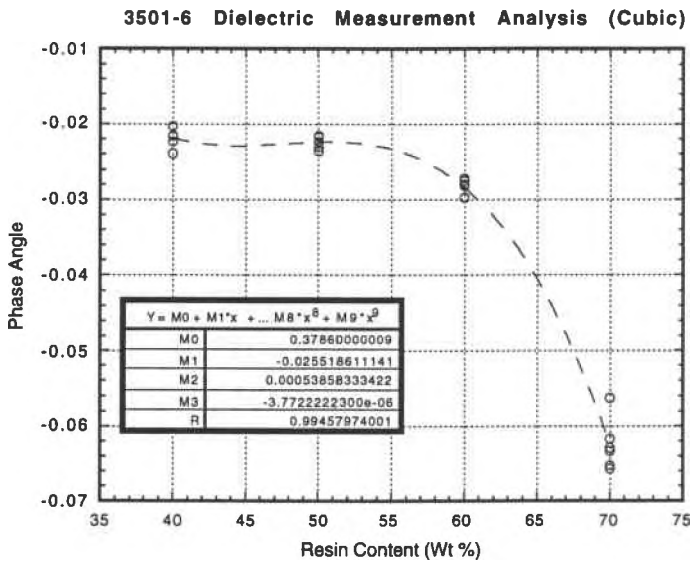

Figure 5.3 Phase Angle Measurements of Epoxy/Acetone Solution

As previously mentioned, the long winding times tended to leave the rollers and pulleys in the winding system gummed up with excess resin. Using a less volatile solvent could preclude this problem from occurring. Unfortunately, the only other compatible solvent widely used was methylethylketone (MEK). The use of this solvent was immediately rejected due to its hazardous nature. Isopropyl alcohol (2 Propanol) was attempted but it was discovered that it was not soluble with epoxy. However, it was found that acetone and 2 propanol were miscible with each other. An attempt was made to use a hybrid solvent containing both. In this case the epoxy would first be dissolved in acetone and the resulting solution would be combined with the alcohol and mixed. The first step in using the hybrid solution was to validate whether the dielectric characteristics followed a similar pattern as before. The experiment using the process monitoring equipment was repeated using the various concentrations of the new solution.

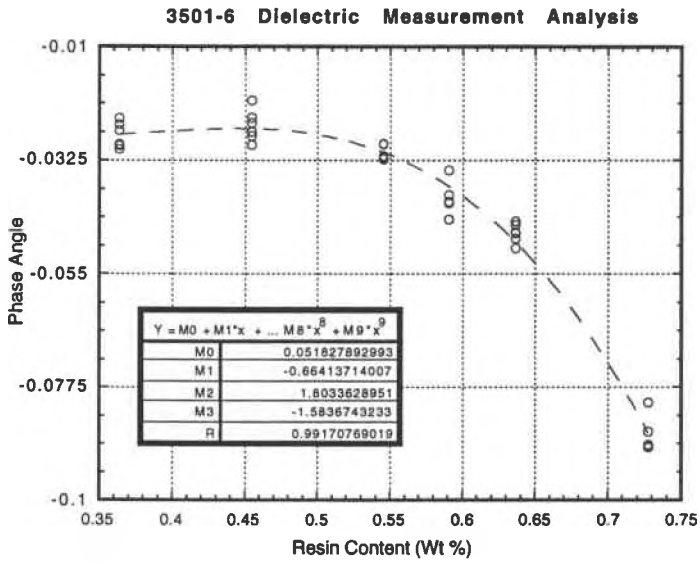

Figure 5.4 Phase Angle Measurements of Epoxy/Acetone/Alcohol Solution

Figure 5.4 shows the same general trend of phase angle change with increased concentration. The important thing to observe from this figure is the data is well behaved. As a result of the dielectric measurements, a procedure was developed for process monitoring during filament winding. A starting value of the solution phase angle was determined by measurement and as the process progressed, additional solvent was added as required in order to keep the dielectric measurement as close as possible to the starting value.

Two factors influenced the choice of the hybrid solvent: the new solvent would be less volatile and it would act as a lubricant. It was believed that changing the volatility would partially eliminate some of the evaporation related problems previously encountered. Additionally, if the solution acted as a lubricant, the tendency of the mechanism to become sticky during the winding process would be eliminated.

An observation made during earlier winding attempts was that some form of mixing had to be accomplished. This would ensure that the an accurate measurement of the dielectric constant of the bulk solution was obtained. A circulation system was designed in order to keep the solution adequately mixed (see Figure 5.5).

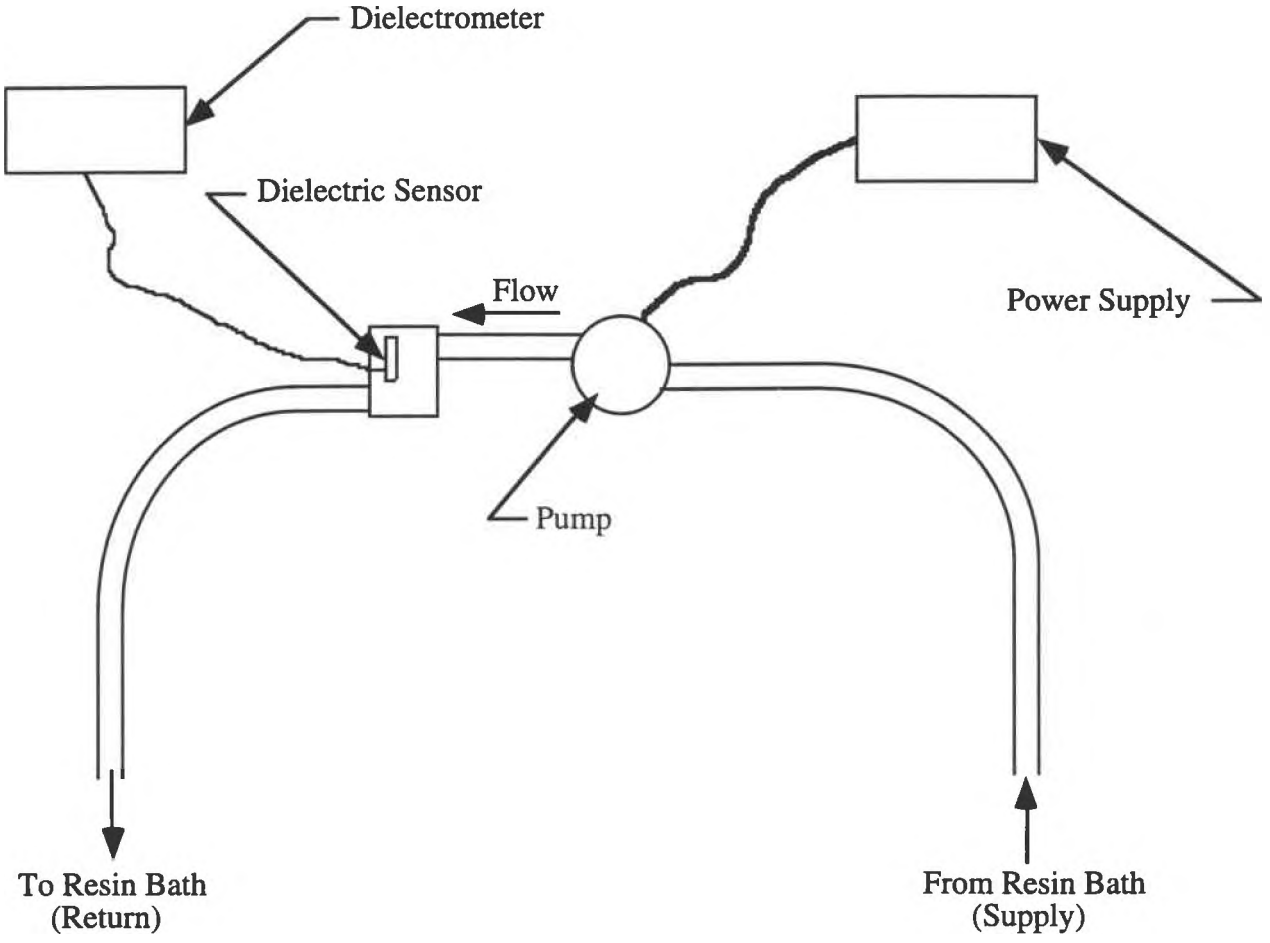

Figure 5.5 Circulation and Dielectric Sensor Systems

A small DC pump and power supply were obtained for this purpose. The circulation/sensor system was designed so the flow of solution out of the pump was directly against the face of the sensor. The flow of solution directly onto the sensor would erode any epoxy film

that might form. This erosion would allow for accurate dielectric measurements and subsequent modification of the solution .

5. FIBER VOLUME REDUCTION THROUGH USE OF HYBRID SOLVENTS:

An attempt was made to determine whether the modification of the solution would cure the fiber volume problem. Two small unidirectional panels were wound, one using the hybrid solution and one with the conventional. Both panels were cured in the autoclave at the same time. Following fabrication, nondestructive and destructive analyses were conducted to see whether the physical characteristics of the materials changed as well as a check to see if the fiber volume was reduced. An important observation during the actual winding was that the hybrid solvents did indeed act as a lubricant. No problems were noticed with sticking as was common with the acetone/epoxy mixture. C-scans showed the debulk process successfully removed the less volatile alcohol, resulting in well compacted laminates with little porosity. Thermomechanical and differential scanning calorimetry analyses were also conducted on samples of panels to determine if the glass transition temperature and the degree of cure were the same in both panels. The results from these tests indicated that upon successfully removing the solvents during the debulk cycle, the resulting polymeric matrix characteristics were identical. Unfortunately the fiber volumes of both remained high indicating that control of the viscosity alone would not cure the problem.

The only other cause for the high fiber volumes was determined to be excessive bleeding of the resin during the initial portion of the cure cycle. The problem with winding a flat mandrel is that it is impossible to adequately construct a dam to restrict the flow of resin during the point of low viscosity during the cure cycle. A perforated nylon release ply had been used and it adequately contained the resin on the flat sides of the mandrel. However, C-scans showed that the regions closest to the mandrel edges were typically dry

due to resin migration. In the absence of adequate resin in these areas, resin would wick from the center of the laminate, ultimately leading to high fiber volumes.

A better method for containing the resin was required. Since the perforated nylon worked well for containing resin on the flat sides of the mandrel, it seemed obvious that some sort of film wrapped continually around the mandrel might work. Additionally, a requirement for the film to be very tight at the mandrel edges existed. At this point it seemed that shrink tape might be the solution. A sample of high temperature shrink tape with a release agent preapplied was obtained and used in the fabrication of yet another group of panels. The use of the shrink tape forced most of the resin to remain in place, thus resulting in laminates with acceptable fiber volumes.

CHAPTER VI

MECHANICAL TESTING

1. LAMINATE STRENGTHS:

Following separation of the laminate from the mandrel, two rectangular panels resulted. For the case of prestressed composites, both of the panels had the same degree of prestress. The specimens were obtained by cutting these panels into 3/4 inch strips. For use during the tests, 14 prestressed and 9 conventional unidirectional coupons were fabricated. There were fewer conventionally processed specimens because some were unusable due to an unacceptable degree of fiber wash. There were also 16 prestressed and 15 conventional crossply specimens fabricated. All of these specimens were quite thin, being from 0.017 to 0.018 inches thick. Coupons of this thickness represent roughly the equivalent of a 4 ply laminate.

All coupons were loaded to failure and the ultimate loads required to break the specimens were recorded.

Table 6.1
Strength of Unidirectional Composites (106 ksi prestress)

	Prestressed	Conventional
Number of Specimens	14	9
Mean Strength (ksi)	288.5	261.5
Standard Deviation (ksi)	21.2	17.5

Table 6.2
Strength of $[0^o/90^o]_s$ Composites (112 ksi prestress)

	Prestressed	Conventional
Number of Specimens	16	15
Mean Strength (ksi)	142.1	122.5
Standard Deviation (ksi)	10.2	12.0

Preceding these tests, the specimen thickness and width were obtained so that the stress in the coupons at failure could be determined. Tables 6.1 and 6.2 contain the mean composite strength and standard deviation of these unidirectional and crossply laminates. As was mentioned previously, the prestress levels for the unidirectional and crossply laminates were approximately 106 and 112 ksi respectively. It is obvious from the data that the prestressed coupons are indeed stronger than the control group.

2. FIRST PLY FAILURE DETERMINATION:

Strain displacement data was also desired but due to the large number of specimens, only certain coupons were strain gaged. These specimens were obtained from the area immediately adjacent to the edges of the rectangular plates (2 strain gaged specimens per panel). In order to determine the point at which first ply failure occurred, a biaxial rosette was installed at the middle of these coupons. Upon conclusion of testing, the output from the transverse gages was observed and the point at which the traces showed significant perturbation from the previously smooth curves was noted. This point was interpreted to correspond to first ply failure. This procedure was validated by subsequent testing in

which an acoustic emission sensor was fastened to a specimen which was also strain gaged. The point at which the gage output first indicated that an event had occurred corresponded to the first significant acoustic response. In order to verify that first ply failure had indeed occurred, the applied load was removed. The specimen was then taken from the load frame and viewed under a microscope where it was observed that first ply failure had occurred.

Table 6.3
First Ply Failure Comparison ($[0^o/90^o]_s$)

	Prestressed	Conventional
Number of Specimens	4	4
Mean Stress at First Ply Failure (ksi)	65.5	43.8
Standard Deviation	12.2	7.4

Table 6.3 contains data obtained from the strain gaged specimens. Observation of the data indicates that as was predicted, the load which induces first ply failure in the prestressed laminates was significantly higher than that seen with the conventionally processed specimens. This data shows agreement with that presented by Schulte and Marrissen [7]. It should be reiterated that only four specimens of each type (prestressed and conventional) were strain gaged and tested. For this reason, the statistical comparison shown above may not be entirely representative of actual composite strengths.

CHAPTER VII

RESULTS AND CONCLUSIONS

1. DISCUSSION:

There were two primary objectives of this research: the first was to demonstrate that thermal residual stresses could be modified so that laminates can be loaded to higher strain levels before any significant damage occurs. The second objective was to determine if the micromechanical fiber/matrix interface stresses could be reduced in order to prevent the process induced cracking seen in ceramic composites. The ability to undergo higher strain levels is important since actual laminate designs are dictated by the strains seen by a structure in service.

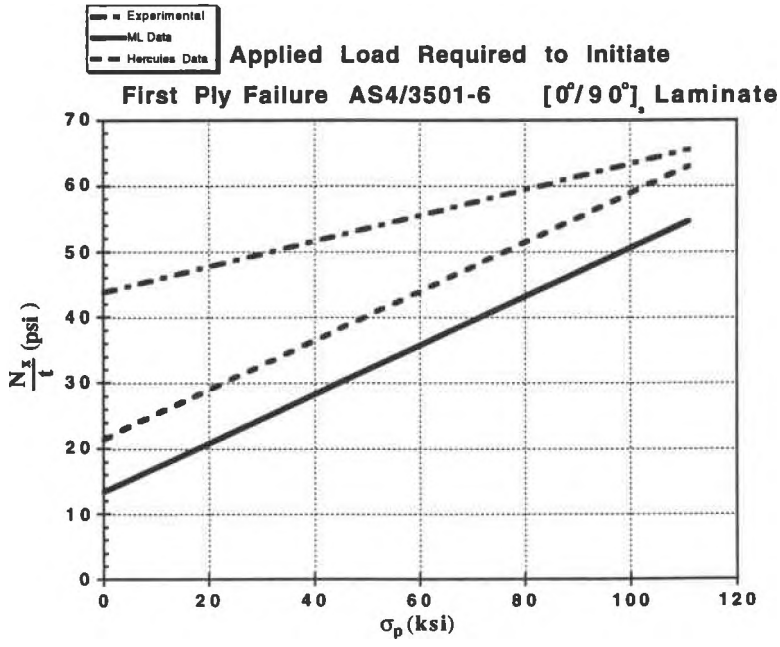

Figure 7.1 Comparison of Experimental and Theoretical First Ply Failure Loads

Figure 7.1 contains the theoretical data that was previously plotted in Figure 4.2 as well the experimental data from Table 6.3. The important thing to note is both methods show the point at which first ply failure occurs can be modified by increasing the stress applied to the fibers during processing. It is obvious from this figure that the predicted and experimental first ply failure points are not the same for a given level of prestress, even when accounting for the bounded theoretical solution. A significant factor in this difference was the fabricated coupons had high fiber volumes (approximately 70%) while the theoretical analysis was conducted assuming a 60% fiber volume which is optimal for a graphite/epoxy composite. A number of attempts were made at trying to reduce the fiber volume and a method previously discussed demonstrated that it could be reduced by using hybrid solvents, process monitoring, and shrink wrapping. However, insufficient quantities of uncured neat epoxy resin prevented additional fabrication and testing.

The slopes of the experimental and theoretical curves also show significant disagreement. These differences may be due to the assumption of values for the fiber transverse modulus, poissons ratio, and the iterated solution for the transverse CTE. Additionally, the analytical model is based upon the assumption of perfect bonding at the fiber/matrix interface. A third potential cause may be that the model is based on the assumption that the stress free temperature is the cure temperature. This assumption is most likely erroneous due to the fact that cure shrinkage stresses are totally neglected. A fourth possibility is that as the mandrel expanded, significant fiber nesting occurred at the ends which relieved some of the prestress. Finally, as mentioned in the last chapter, only four specimens of each type were strain gaged and tested. As a result, the first ply failure loads plotted may be somewhat erroneous due to an insufficient number of specimens to make a statistically accurate comparison.

As shown by the results of the unidirectional tensile tests (Table 6.1), the prestressed coupons showed an increase in strength when compared to the control group. This

observation agrees with that made by Jorge, Marques, and De Castro [2]. However, inspection of the standard deviation indicates the statistical improvement in the variability of composite strengths as predicted by Manders and Chou [1] is not seen, at least for these specimens. The cause of this disagreement is unknown. A look at the same data for the crossply laminates (Table 6.2) indicates that the variability in strengths does show reduction in the prestressed laminates. It is interesting to note that the strengths of these laminates also showed significant improvements over those obtained from the control group. It seems logical to conclude that the strength increase seen in these laminates is due to improvements in unidirectional composite strength. It is presently unknown whether the unidirectional strength increases seen are due solely to the elimination of the fiber flaws as postulated by Manders and Chou or if other factors such as the modification of the residual stresses or improved fiber alignment may be of importance. Inspection of prestressed and conventional coupons under a microscope reveals exactly what would be expected, that prestressed composites have fibers which are significantly straighter than is typically seen in conventional composites. The effect of fiber waviness has been proposed as a possible cause of poor compression strength in composites [13] but the possibility exists that fiber alignment may play a role in tensile strengths as well.

2. POSSIBLE FUTURE WORK:

The modification and reduction of matrix residual stresses has the potential to offer benefits other than increased tensile strengths. These other benefits could include improvements in both fatigue life, impact resistance and compression strength. There was some work attempted in compression testing of prestressed laminates using the technique developed by Kim and Crasto [12]. Unfortunately, these tests were conducted prior to the establishment of an adequate fabrication technique. Since it was hard to fabricate panels with consistent thickness, sandwich specimens with face sheets of different thickness

resulted. These specimens showed poor compression results, primarily due to the fact that one face sheet always buckled prematurely.

Wet winding of flat plates was chosen due to ease as well as availability of equipment. However, the technique is not without its problems. The setup used to apply tension to the fibers caused visible damage to the tow which could have impact on the variability of composite strengths. For this reason any future work such as fatigue, impact, or additional compression testing should be done with better quality panels. Tape winding would have provided much better panels but could not be performed for this effort due to the unavailability of adequate equipment.

Another area to explore would be in the fabrication of prestressed brittle matrix composites. A large number of processing issues would have to be resolved prior to establishing a successful technique. However, the analysis done in Chapter 3 indicates that the application of relatively low stresses during the fabrication of these materials has the potential of vastly modifying the residual stresses and in doing so, possibly allowing for damage free composites.

The overall objective of this research was to both demonstrate the ability to prestress composite materials, especially laminates in which the fibers are applied in more than one direction. The second objective was to show that modifying the residual stresses would result in improved composite performance. Irrespective of the fact that problems with composite quality had occurred, both objectives were met.

APPENDIX I

CROSSPLY LAMINATE CALCULATIONS

From Jones, the reduced stiffnesses in terms of engineering constants are

$$Q_{11} = \frac{E_1}{1-\nu_{12}\nu_{21}} \tag{A.1}$$

$$Q_{12} = \frac{\nu_{12}E_2}{1-\nu_{12}\nu_{21}} = \frac{\nu_{21}E_1}{1-\nu_{12}\nu_{21}} \tag{A.2}$$

$$Q_{22} = \frac{E_2}{1-\nu_{12}\nu_{21}} \tag{A.3}$$

$$Q_{66} = G_{12} \tag{A.4}$$

where $$\frac{\nu_{12}}{E_1} = \frac{\nu_{21}}{E_2} \tag{A.5}$$

The laminate extensional stiffnesses are

$$A_{ij} = \sum_{k=1}^{N} (Q_{ij}^{(k)})(z_k - z_{k-1}) \qquad i,j=1,2,6 \tag{A.6}$$

where k represents the ply number and the z's are as indicated in Figure A.1

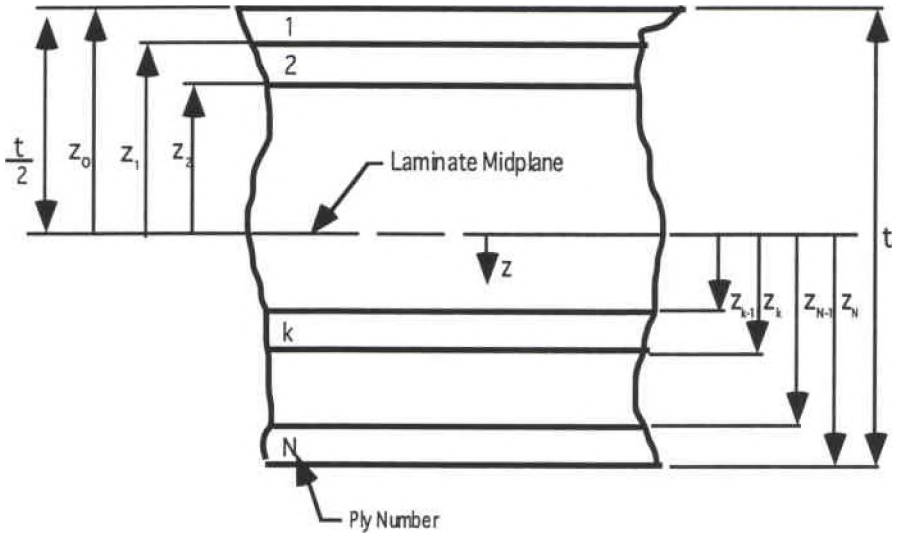

Figure A.1 Geometry of an N-Ply Laminate

The following material properties represent those found in AS-4/3501-6

$E_1 = 20 \times 10^6$ psi $\quad E_2 = 1.5 \times 10^6$ psi $\quad G_{12} = 0.8 \times 10^6$ psi $\quad \nu_{12} = 0.3$

with

$$\nu_{21} = \frac{(.3)(1.5 \times 10^6)}{(20 \times 10^6)} = 0.0225$$

along with the associated failure strengths

$X_t = X_c = 300$ ksi $\quad Y_t = 7.5$ ksi $\quad Y_c = 30$ ksi

As specified in Chapter 3, two sets of lamina thermal expansion data are used in order to bound the solution. For the specific case of a 4 layer crossply laminate, the transformed reduced ply stiffnesses are calculated using equations A.1 - A.5

$$Q_{11}^{(1)} = Q_{11}^{(4)} = \frac{20 \times 10^6}{1-(.3)(.0225)} = 20.1359 \times 10^6 \text{ psi}$$

$$Q_{11}^{(2)} = Q_{11}^{(3)} = \frac{1.5 \times 10^6}{1-(.3)(.0225)} = 1.5102 \times 10^6 \text{ psi}$$

$$Q_{12} = \frac{(.3)(1.5 \times 10^6)}{1-(.3)(.0225)} = 0.4531 \times 10^6 \text{ psi} \quad \text{(all plies)}$$

$$Q_{22}^{(1)} = Q_{22}^{(4)} = \frac{1.5 \times 10^6}{1-(.3)(.0225)} = 1.5102 \times 10^6 \text{ psi}$$

$$Q_{22}^{(2)} = Q_{22}^{(3)} = \frac{20 \times 10^6}{1-(.3)(.0225)} = 20.1359 \times 10^6$$

$$Q_{66}^{(1)} = Q_{66}^{(2)} = Q_{66}^{(3)} = Q_{66}^{(4)} = G_{12} = 0.8 \times 10^6 \text{ psi}$$

The extensional stiffnesses (equations A.6) for the same laminate are as follows:

$$\begin{aligned} A_{11} = A_{22} &= Q_{11}^{(1)}\left(\frac{t}{4}\right)+Q_{11}^{(2)}\left(\frac{t}{4}\right)+Q_{11}^{(3)}\left(\frac{t}{4}\right)+Q_{11}^{(4)}\left(\frac{t}{4}\right) \\ &= 2Q_{11}^{(1)}\left(\frac{t}{4}\right)+2Q_{11}^{(2)}\left(\frac{t}{4}\right) \\ &= (Q_{11}^{(1)} + Q_{11}^{(2)})\left(\frac{t}{2}\right) \end{aligned} \qquad \text{(A.7)}$$

Similarly, the remaining extensional stiffnesses are

$$A_{12} = (Q_{12}^{(1)} + Q_{12}^{(2)})\left(\frac{t}{2}\right) = Q_{12}t \qquad \text{(A.8)}$$

$$A_{22} = (Q_{22}^{(1)} + Q_{22}^{(2)})(\frac{t}{2})$$
$$A_{66} = Q_{66}^{(1)}\, t = G_{12}t \qquad (A.9)$$

Substituting in the previously determined transformed reduced stiffnesses yields

$$A_{11} = A_{22} = (20.1359 \times 10^6 + 1.5102 \times 10^6)(\frac{t}{2})$$
$$= 10.8231 \times 10^6 t \text{ psi}$$

$$A_{12} = (0.4531 \times 10^6 + 0.4531 \times 10^6)(\frac{t}{2})$$
$$= 0.4531 \times 10^6 t \text{ psi}$$

$$A_{66} = 0.8 \times 10^6 t \text{ psi}$$

$$A_{16} = A_{26} = 0$$

Where t is the laminate thickness. The inverted laminate extensional stiffnesses are

$$A'_{11} = A'_{22} = 0.09256 \times 10^{-6}/(t \text{ psi})$$

$$A'_{12} = -.00387 \times 10^{-6}/(t \text{ psi})$$

$$A'_{66} = 1.25000 \times 10^{-6}/(t \text{ psi})$$

the fictitious thermal equivalent loads can be determined from equations 4.7

$$\begin{bmatrix} N_x^T \\ N_y^T \\ N_{xy}^T \end{bmatrix} = \int \begin{bmatrix} Q_{11} & Q_{12} & 0 \\ Q_{12} & Q_{22} & 0 \\ 0 & 0 & Q_{66} \end{bmatrix}_k \begin{bmatrix} \varepsilon_x^T \\ \varepsilon_y^T \\ \gamma_{xy}^T \end{bmatrix}_k dz \tag{A.10}$$

Where for a 4 layer crossply laminate, $Q_{16}=Q_{26}=0$. Upon integrating, expanding, assuming that the applied strains due to prestressing are equivalent to Equations 4.14, and setting $\varepsilon_{xy}^T = 0$ (all plies) yields the following expression for the fictitious prestress forces

$$\begin{aligned} N_x^T = {} & (Q_{11}^{(1)}\bar{\alpha}_1 + Q_{12}^{(1)}\bar{\alpha}_2)\Delta T_2\frac{t}{4} + (Q_{11}^{(2)}\bar{\alpha}_2 + Q_{12}^{(2)}\bar{\alpha}_1)\Delta T_2\frac{t}{4} \\ & + (Q_{11}^{(3)}\bar{\alpha}_2 + Q_{12}^{(3)}\bar{\alpha}_1)\Delta T_2\frac{t}{4} + (Q_{11}^{(4)}\bar{\alpha}_1 + Q_{12}^{(4)}\bar{\alpha}_2)\Delta T_2\frac{t}{4} \end{aligned} \tag{A.11}$$

$$\begin{aligned} N_y^T = {} & (Q_{12}^{(1)}\bar{\alpha}_1 + Q_{22}^{(1)}\bar{\alpha}_2)\Delta T_2\frac{t}{4} + (Q_{12}^{(2)}\bar{\alpha}_2 + Q_{22}^{(2)}\bar{\alpha}_1)\Delta T_2\frac{t}{4} \\ & + (Q_{12}^{(3)}\bar{\alpha}_2 + Q_{22}^{(3)}\bar{\alpha}_1)\Delta T_2\frac{t}{4} + (Q_{12}^{(4)}\bar{\alpha}_1 + Q_{22}^{(4)}\bar{\alpha}_2)\Delta T_2\frac{t}{4} \end{aligned} \tag{A.12}$$

$$N_{xy}^T = 0 \tag{A.13}$$

In the case of a symmetric laminate

$$\begin{aligned} Q_{11}^{(1)} &= Q_{11}^{(4)} \quad Q_{11}^{(2)} = Q_{11}^{(3)} \\ Q_{12}^{(1)} &= Q_{12}^{(4)} \quad Q_{12}^{(2)} = Q_{12}^{(3)} \\ Q_{66}^{(1)} &= Q_{66}^{(2)} = Q_{66}^{(3)} = Q_{66}^{(4)} \end{aligned}$$

which results in

$$N_x^T = \frac{1}{2}\left[(Q_{11}^{(1)} + Q_{12}^{(2)})\bar{\alpha}_1 + \frac{1}{2}(Q_{12}^{(1)} + Q_{11}^{(2)})\bar{\alpha}_2)\right]\Delta T_2 t \tag{A.14}$$

Similarly

$$N_y^T = \frac{1}{2}\left[(Q_{12}^{(1)} + Q_{22}^{(2)})\bar{\alpha}_1 + \frac{1}{2}(Q_{22}^{(1)} + Q_{12}^{(2)})\bar{\alpha}_2)\right]\Delta T_2 t \tag{A.15}$$

$$N_{xy}^{T} = 0 \tag{A.16}$$

Equations A.1 - A.5 along with the data found in Tables 4.3 and 4.4 are used to calculate the fictitious preload forces. These forces are listed in Table A.1.

Table A.1
Fictitious Preload Forces

	$\frac{N_x^T}{t} = \frac{N_x^T}{t}$ (psi)	
σ_p (ksi)	Hercules	ML
0	-3.22	-2.91
50	-17.7	-17.4
106	-34.2	-33.8
112	-35.6	-35.3
150	-46.7	-46.4
200	-61.3	-60.9
250	-75.8	-75.5
300	-90.2	-90.0
350	-104.7	-104.5

The next step is to determine the load which will initiate first ply failure. As stated in Chapter 4, the maximum stress failure criterion was chosen due to its ease of use. This load is determined by rewriting Equation 4.16 and substituting the required data. For the case being solved, N_y is set equal to zero due to the applied load being uniaxial tension. Additionally, σ_x is specified to be the lamina transverse tensile strength, Y. This allows the expression to be simplified with the result being Equation A.17.

$$N_x = \frac{\left(Y - Q_{11}^{(2)}\left[A'_{11}N_x^T + A'_{12}N_y^T - \bar{\alpha}_2\Delta T_2\right] - Q_{12}^{(2)}\left[A'_{12}N_x^T + A'_{22}N_y^T - \bar{\alpha}_1\Delta T_2\right]\right)}{Q_{11}^{(2)}A'_{11} + Q_{12}^{(2)}A'_{12}} \qquad (A.17)$$

A FORTRAN program was written to solve for the effective coefficients of thermal expansion using the concentric cylinder model. These coefficients as shown in Tables 4.3 and 4.4 are used with the previously determined transformed reduced stiffnesses, extensional stiffnesses, and the fictitious forces to solve for the load required to initiate first ply failure. Table A.2 lists these loads as a function of the applied prestress.

Table A.2
Maximum Applied Load (N_x)

	$\frac{N_x}{t}$ (psi)	
σ_p (ksi)	Hercules	ML
0	21.5	13.4
50	40.0	31.9
106	61.1	52.8
112	63.0	54.7
150	77.1	69.0
200	95.6	87.5
250	114.1	106.0
300	132.7	124.6
350	151.2	143.1

Tables A.3 and A.4 contain the ply stresses present at first ply failure. The second ply values for σ_x indicate that the values were calculated properly since they are all the same and are equal to the lamina transverse tensile strength.

Table A.3
Ply Stresses at First Ply Failure (Hercules Data)

σ_p (ksi)	$\sigma_x^{(1)}$ (ksi)	$\sigma_y^{(1)}$ (ksi)	$\sigma_x^{(2)}$ (ksi)	$\sigma_y^{(2)}$ (ksi)
0	35.5	5.3	7.5	-5.3
50	72.6	3.4	7.5	-3.4
106	114.7	1.3	7.5	-1.3
112	118.4	1.1	7.5	-1.1
150	146.7	-.36	7.5	.36
200	183.7	-2.2	7.5	2.2
250	220.8	-4.1	7.5	4.1
300	257.8	-6.0	7.5	6.0
350	294.9	-7.9	7.5	7.9

Table A.4
Ply Stresses at First Ply Failure (ML Data)

σ_p (ksi)	$\sigma_x^{(1)}$ (ksi)	$\sigma_y^{(1)}$ (ksi)	$\sigma_x^{(2)}$ (ksi)	$\sigma_y^{(2)}$ (ksi)
0	19.3	6.1	7.5	-6.1
50	56.3	4.2	7.5	-4.2
106	98.1	2.1	7.5	-2.1
112	102.0	1.9	7.5	-1.9
150	130.5	.47	7.5	-.47
200	167.5	-1.4	7.5	1.4
250	204.6	-3.3	7.5	3.3
300	241.6	-5.2	7.5	5.2
350	278.7	-7.1	7.5	7.1

APPENDIX II

PARAMETRIC STUDY

Since transverse fiber properties are unknown, then an attempt to determine the unknown properties was made using a parametric analysis with known constituent properties, laminate properties, and the analytical model (concentric cylinder). It was hoped that by varying the unknown material properties used during the analysis, a convergence with known lamina properties would occur. The problem with this approach was that there were three unknown transverse fiber properties: the modulus, poissons ratio, and CTE. In order to proceed, it was decided to assume values for two of the unknown properties and vary the third in order to determine if the transverse laminate CTE obtained analytically was sensitive to changes in the parameter being varied.

I will start with known values

$E_1^f = 34.0 \times 10^6$ psi
$\nu_{12}^f = 0.3$
$E^m = 0.62 \times 10^6$ psi
$\nu^m = 0.34$
$\alpha^m = 22.8 \times 10^{-6}$ in/in ^oF

I was told by Hercules that $\alpha_2^f = 10.0 \times 10^{-6}$ in/in ^oF (a number that appears to be in error). However, I will start with this value and use the analytical model in order to converge on a solution which actually matches laminate thermal properties.

In order to proceed with the convergence analysis, I'll assume $E_2^f = 2.4 \times 10^6$ psi and vary ν_{23}^f from .25 to .55. I will observe the cylinder hoop strain at the outer radius of the matrix cylinder. This strain should correspond (match) the transverse lamina thermal strain ($\alpha\Delta T$). Additionally, the parametric study will start with lamina properties from Hercules

$\alpha_1 = -0.044 \times 10^{-6}$ in/in °F
$\alpha_2 = 12.0 \times 10^{-6}$ in/in °F

with $\Delta T = -280$°F, the lamina thermal transverse strain should be

$$\varepsilon_2^{lamina} = (-280°F)(12 \times 10^{-6} \text{ in/in } °F) = -3.36 \times 10^{-3} \text{ in/in}$$

I also should note that the longitudinal strain predicted by the model also should correspond to the lamina thermal longitudinal strain

$$\varepsilon_1^{lamina} = (-280°F)(-0.044 \times 10^{-6} \text{ in/in } °F) = 1.232 \times 10^{-5} \text{ in/in}$$

The following data corresponds to the case where ν_{23}^f is varied while holding all other variables fixed.

$\nu_{23}^f = .25$
$\varepsilon_1 =$ 1.032768589785000E-005
$\varepsilon_2 =$ -4.891242380810373E-003

$\nu_{23}^f = .3$
$\varepsilon_1 =$ 1.032151702557590E-005
$\varepsilon_2 =$ -4.879884398937760E-003

$\nu_{23}^f = .35$
$\varepsilon_1 =$ 1.031530982923320E-005
$\varepsilon_2 =$ -4.868455855786750E-003

$\nu_{23}^f = .4$
$\varepsilon_1 = 1.030906394319552E-005$
$\varepsilon_2 = -4.856956078015810E-003$

$\nu_{23}^f = .45$
$\varepsilon_1 = 1.030277901208680E-005$
$\varepsilon_2 = -4.845384411367590E-003$

$\nu_{23}^f = .5$
$\varepsilon_1 = 1.029645466103230E-005$
$\varepsilon_2 = -4.833740165702540E-003$

$\nu_{23}^f = .55$
$\varepsilon_1 = 1.029009052186981E-005$
$\varepsilon_2 = -4.822022663040940E-003$

I will now set $\nu_{23}^f = .55$ and vary E_2^f from 1.5 to 2.4 x 10^6 psi

$E_2^f = 1.5 \times 10^6$ psi
$\varepsilon_1 = 1.032398915243380E-005$
$\varepsilon_2 = -4.884436020480610E-003$

$E_2^f = 1.6 \times 10^6$ psi
$\varepsilon_1 = 1.031841823883231E-005$
$\varepsilon_2 = -4.874178986000180E-003$

$E_2^f = 1.7 \times 10^6$ psi
$\varepsilon_1 = 1.031347683358601E-005$
$\varepsilon_2 = -4.865080987422191E-003$

$E_2^f = 1.8 \times 10^6$ psi
$\varepsilon_1 = 1.030906394197890E-005$
$\varepsilon_2 = -4.856956075723900E-003$

$E_2^f = 1.9 \times 10^6$ psi
$\varepsilon_1 = 1.030509907667780E-005$
$\varepsilon_2 = -4.849656059462180E-003$

$E_2^f = 2.0 \times 10^6$ psi
$\varepsilon_1 = 1.030151730399543E-005$
$\varepsilon_2 = -4.843061384255872E-003$

$E_2^f = 2.1 \times 10^6$ psi
$\varepsilon_1 =$ 1.029826566002410E-005
$\varepsilon_2 =$ -4.837074534157022E-003

$E_2^f = 2.2 \times 10^6$ psi
$\varepsilon_1 =$ 1.029530051386980E-005
$\varepsilon_2 =$ -4.831615177210560E-003

$E_2^f = 2.3 \times 10^6$ psi
$\varepsilon_1 =$ 1.029258559893641E-005
$\varepsilon_2 =$ -4.826616540025020E-003

$E_2^f = 2.4 \times 10^6$ psi
$\varepsilon_1 =$ 1.029009052186981E-005
$\varepsilon_2 =$ -4.822022663040940E-003

I will now set ν_{23}^f to .55 and E_2^f to 2.4 x 10^6 psi and vary α_2^f starting from 10.0 x 10^{-6} in/in ^oF downwards until I reach the proper value which allows convergence of the theoretical and experimental transverse thermal strain

$\alpha_2^f = 10.0 \times 10^{-6}$ in/in ^oF
$\varepsilon_1 =$ 1.029009052186981E-005
$\varepsilon_2 =$ -4.822022663040940E-003

$\alpha_2^f = 9.0 \times 10^{-6}$ in/in ^oF
$\varepsilon_1 =$ 1.019180946295550E-005
$\varepsilon_2 =$ -4.641069900130660E-003

$\alpha_2^f = 8.0 \times 10^{-6}$ in/in ^oF
$\varepsilon_1 =$ 1.009352831465500E-005
$\varepsilon_2 =$ -4.460116972644711E-003

$\alpha_2^f = 7.0 \times 10^{-6}$ in/in ^oF
$\varepsilon_1 =$ 9.995247211047500E-006
$\varepsilon_2 =$ -4.279164127446600E-003

$\alpha_2^f = 6.0 \times 10^{-6}$ in/in ^oF
$\varepsilon_1 =$ 9.896966107440043E-006
$\varepsilon_2 =$ -4.098211282248490E-003

$\alpha_2^f = 5.0 \times 10^{-6}$ in/in °F
$\varepsilon_1 =$ 9.798684959139461E-006
$\varepsilon_2 =$ -3.917258354762540E-003

$\alpha_2^f = 4.0 \times 10^{-6}$ in/in °F
$\varepsilon_1 =$ 9.700403855532010E-006
$\varepsilon_2 =$ -3.736305509564430E-003

$\alpha_2^f = 3.0 \times 10^{-6}$ in/in °F
$\varepsilon_1 =$ 9.602122751924553E-006
$\varepsilon_2 =$ -3.555352664366314E-003

$\alpha_2^f = 2.0 \times 10^{-6}$ in/in °F
$\varepsilon_1 =$ 9.503841625970560E-006
$\varepsilon_2 =$ -3.374399778024284E-003

(Rough convergence with lamina properties provided by Hercules).

Since I have demonstrated that the transverse thermal lamina strain is insensitive to changes in E_2^f and ν_{23}^f, for the parametric study using ML data, I will set ν_{23}^f=.55, E_2^f=2.4 x 10^6 psi, and vary α_2^f from 10.0 x 10^{-6} °F down until convergence with the lamina transverse thermal strain is established.

lamina properties from ML

$\alpha_1 = -0.4 \times 10^{-6}$ in/in°F
$\alpha_2 = 15 \times 10^{-6}$ in/in°F

with ΔT= -280 °F, the thermal transverse strain, ε_2^{lamina}, should be

$$(-280)(15.0 \times 10^{-6} \text{ in/in °F}) = -4.2 \times 10^{-3} \text{ in/in}$$

I also should note that the longitudinal strain predicted by the model also should correspond to the lamina thermal longitudinal strain, ε_1^{lamina}.

$$(-280°F)(-0.4 \times 10^{-6} \text{ in/in °F}) = 1.12 \times 10^{-4} \text{ in/in}$$

α_2^f = 10.0 x 10^{-6} in/in °F
ε_1 = 1.099586731619050E-004
ε_2 = -4.833776459054100E-003

α_2^f = 9.0 x 10^{-6} in/in °F
ε_1 = 1.098603921029903E-004
ε_2 = -4.652823696143822E-003

α_2^f = 8.0 x 10^{-6} in/in °F
ε_1 = 1.097621109546900E-004
ε_2 = -4.471870768657874E-003

α_2^f = 7.0 x 10^{-6} in/in °F
ε_1 = 1.096638298510823E-004
ε_2 = -4.290917923459761E-003

α_2^f = 6.0 x 10^{-6} °F
ε_1 = 1.095655487474750E-004
ε_2 = -4.109965078261650E-003

(Rough convergence with lamina properties provided by ML).

REFERENCES

1. Manders, P.W. and Chou, T.W., "Enhancement of Strength in Composites Reinforced with Previously-Stressed Fibers", Journal of Composite Materials, Vol. 17 (January1983), pp 26-44.

2. Jorge, L.D.A., Marques, A.T., and De Castro, P.M.S.T., "The Influence of Prestressing on the Mechanical Behavior of Uni-Directional Composites", Proccedings of the Fourth European Conference on Composite Materials", (Stuttgart 1990), pp 897-902.

3. Chi, Z. and Chou, T.W., "An Experimental Study of the Effect Of Prestressed Loose Carbon Strands on Composite Strength", Journal of Composite Materials, Vol. 17 (May1983), pp 196-209.

4. Mills, G.J., Brown, G. and Waterman, D., "Prestressing of Fiber/Resin Prepreg Systems for Laminate Property Improvements," Proceedings of the 1975 International Conference on Composite Materials, Vol. 2, (Geneva 1976) pp. 222-246.

5. Mills, G.J. and Dauksys, R.J., "Effects of Prestressing Boron/Epoxy Prepreg on Composite Strength Properties," AIAA Journal, 11, 1459, (1973).

6. Tuttle, M. E., "A Mechanical/Thermal Analysis of Prestressed Composite Laminates", Journal of Composite Materials, Vol. 22 (August1988), pp 780-792.

7. Schulte, K. and Marissen, R., "Influence of Artificial Pre-stressing During Curing of CFRP Laminates on Interfiber Transverse Cracking", Composite Science and Technology, Vol. 44 (1992), pp 361-367.

8. Jones, R.M., "Mechanics of Composite Materials", New York, Hemisphere Publishing Corp., (1975).

9. Hashin, Z. and Rosen, B.W., "The Elastic Moduli of Fiber-Reinforced Materials", Journal of Applied Mechanics, Vol. 31 (1964), pg 223.

10. Timoshenko, S. and Goodier, J.N., "Theory of Elasticity",New York, McGraw-Hill, (1951)

11. Crasto, A.S. and Kim, R.Y., "On the Determination of Residual Stresses in Fiber-Reinforced Thermoset Composites", Proceedings of the American Society for Composites, Seventh Technical Conference (1992), pgs 181-190

12. Kim, R.Y. and Crasto, A.S., "A Longitudinal Compression Test for Composites Using a Sandwich Specimen", Journal of Composite Materials, Vol. 26, No 13 (1992), pp 1915-1929.

13. Highsmith, A.L., Davis, J.J., and Helms, K.L.E.,"The Influence of Fiber Waviness on the Compressive Behavior of Unidirectional Continuous Fiber Composites", Composite Materials: Testing and Design (Tenth Volume), ASTM STP 1120 (1992), pp 20-36